Realization of Unusual Ligand Binding Motifs in Metalated Container Molecules: Synthesis, Structures, and Magnetic Properties of the Complexes $[(L^{Me})Ni_2(\mu\text{-}L')]^{n+}$ with $L' = NO_3^-$, NO_2^-, N_3^-, N_2H_4, Pyridazine, Phthalazine, Pyrazolate, and Benzoate

Julia Hausmann,[a, d] Marco H. Klingele,[a, d] Vasile Lozan,[a] Gunther Steinfeld,[a] Dieter Siebert,[b] Yves Journaux,[c] Jean Jacques Girerd,[c] and Berthold Kersting*[a]

Abstract: A series of dinickel(II) complexes with the 24-membered macrocyclic hexaazadithiophenol ligand H_2L^{Me} was prepared and examined. The doubly deprotonated form $(L^{Me})^{2-}$ forms complexes of the type $[(L^{Me})Ni_2^{II}(\mu\text{-}L')]^{n+}$ with a bioctahedral $N_3Ni^{II}(\mu\text{-}SR)_2(\mu\text{-}L')Ni^{II}N_3$ core and an overall calixarene-like structure. The bridging coordination site L′ is accessible for a wide range of exogenous coligands. In this study $L' = NO_3^-$, NO_2^-, N_3^-, N_2H_4, pyrazolate (pz), pyridazine (pydz), phthalazine (phtz), and benzoate (OBz). Crystallographic studies reveal that each substrate binds in a distinct fashion to the $[(L^{Me})Ni_2]^{2+}$ portion: NO_2^-, N_2H_4, pz, pydz, and phtz form $\mu_{1,2}$-bridges, whereas NO_3^-, N_3^-, and OBz^- are $\mu_{1,3}$-bridging. These distinctive binding motifs and the fact that some of the coligands adopt unusual conformations is discussed in terms of complementary host–guest interactions and the size and form of the binding pocket of the $[(L^{Me})Ni_2]^{2+}$ fragment. UV/Vis and electrochemical studies reveal that the solid-state structures are retained in the solution state. The relative stabilities of the complexes indicate that the $[(L^{Me})Ni_2]^{2+}$ fragment binds anionic coligands preferentially over neutral ones and strong-field ligands over weak-field ligands. Secondary van der Waals interactions also contribute to the stability of the complexes. Intramolecular ferromagnetic exchange interactions are present in the nitrito-, pyridazine-, and the benzoato-bridged complexes where $J = +6.7$, $+3.5$, and $+5.8\ cm^{-1}$ ($\mathbf{H} = -2J\mathbf{S}_1\mathbf{S}_2$, $S_1 = S_2 = 1$) as indicated by magnetic susceptibility data taken from 300 to 2 K. In contrast, the azido bridge in $[(L^{Me})Ni_2(\mu_{1,3}\text{-}N_3)]^+$ results in an antiferromagnetic exchange interaction $J = -46.7\ cm^{-1}$. An explanation for this difference is qualitatively discussed in terms of bonding differences.

Keywords: activation of small molecules · bimetallic reactivity · macrobinucleating ligands · magnetic properties · nickel

Introduction

The coordination chemistry of transition-metal complexes with well-defined binding pockets is currently attracting much interest.[1–5] By adjusting the size and form of the pocket it is often possible to coordinate coligands in unusual coordination modes, to activate and transform small molecules,[6] or to stabilize reactive intermediates.[7] Such compounds also allow an interplay of molecular recognition and transition-metal catalysis,[8,9] and the construction of more effective enzyme mimics.[10] Consequently, a large number of supporting ligands have been developed that create confined environments about active metal coordination sites. The majority of these ligands form mononuclear compounds, as for instance the calixarenes,[11] the cyclodextrins,[12,13] and some tripod ligands.[14,15] In contrast, there are only a few ligand systems that impose cagelike structures about polynuclear cores.[16–18] Polyazadithiophenolate macrocycles[19,20] of the

[a] Dipl.-Chem. J. Hausmann, M. H. Klingele, Dr. V. Lozan, Dipl.-Chem. G. Steinfeld, Priv.-Doz. Dr. B. Kersting
Institut für Anorganische und Analytische Chemie
Universität Freiburg
Albertstrasse 21, 79104 Freiburg (Germany)
Fax: (+49) 761-203-5987
E-mail: berthold.kersting@ac.uni-freiburg.de

[b] Prof. D. Siebert
Institut für Physikalische Chemie, Universität Freiburg
Albertstrasse 23a, 79104 Freiburg (Germany)

[c] Dr. Y. Journaux, Prof. J. J. Girerd
Laboratoire de Chimie Inorganique, CNRS-Université Paris-Sud
Bat 420, 91405 Orsay (France)

[d] Dipl.-Chem. J. Hausmann, M. H. Klingele
Present address: Department of Chemistry, University of Otago, PO Box 56, Dunedin (New Zealand)

Supporting information for this article is available on the WWW under http://www.chemeurj.org/ or from the author.

DOI: 10.1002/chem.200305705

Robson-type[21–23] readily form dinuclear metal complexes with first-row transition-metal ions. The reduced forms can be functionalized at the secondary amine functions, and, therefore, could be suitable to construct such species.[24]

We have recently investigated the coordination chemistry of the 24-membered macrocyclic hexaazadithiophenolate ligand H_2L^H and its permethylated derivative H_2L^{Me} (Scheme 1).[25] The two macrocycles generate $[(L^R)M^{II}_2]^{2+}$ complex fragments that bind additional coligands L′ to give bioctahedral complexes of the type A or B.[26] In these complexes, the bridging coligands are situated in the hydrophobic pocket of the $[(L^{Me})M_2]^{2+}$ unit made up of the *N*-alkyl residues and the aryl rings of the supporting hexaazadithiophenolate macrocycles. These complexes are amongst the first prototypes for dinuclear complexes with confined binding cavities.[27]

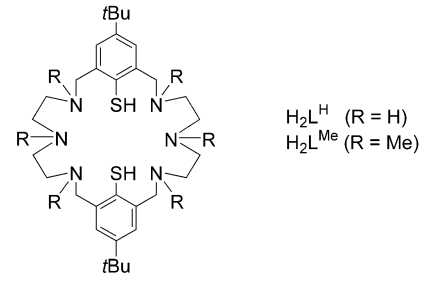

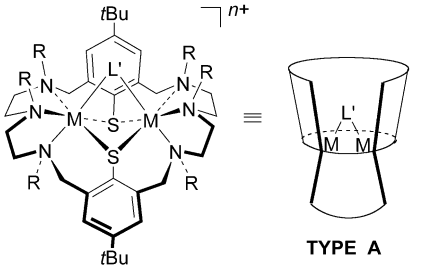

$[(L^R)M_2(\mu\text{-}L')]^{n+}$, M = Ni^{2+}, Co^{2+}; L' = Cl^-, OH^-; *n* = 1

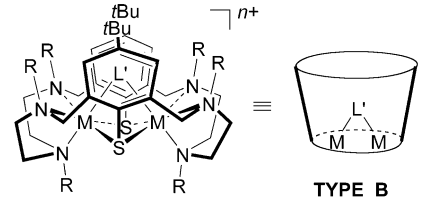

$[(L^R)M_2(\mu\text{-}L')]^{n+}$, M = Ni^{2+}, Co^{2+}; L' = RCO_2^-; *n* = 1

Scheme 1. Structure of the ligands (H_2L^R) and schematic representation of the structures of their corresponding metal complexes $[(L^R)M_2(\mu\text{-}L')]^{n+}$. The cavity representation of the ligand $(L^R)^{2-}$ should not be confused with the one used for cyclodextrins.

From previous work it is clear that the presence of the substituents on the nitrogen donors influences the coordination chemistry of the corresponding complexes significantly. For example, utilization of the permethylated derivative in place of the parent compound H_2L^H drastically alters the ease of the substitution of the bridging halide ions in the chloro-bridged $[(L^R)Ni_2(\mu\text{-}Cl)]^+$ compounds.[28] Likewise, the remarkable ability to fix and transform small molecules such as H_2O and CO_2 is restricted to complexes of the permethylated macrocycle.[29] More recently, the aryl rings of H_2L^{Me} have been demonstrated to influence the stereochemical course of substrate transformations, as for instance the highly diastereoselective *cis*-bromination of α,β-unsaturated carboxylate groups.[30]

So far, our studies have been confined to complexes bearing only three different coligands, namely chloride, hydroxide, and acetate. We have now examined the capability of the $[(L^{Me})Ni_2]^{2+}$ fragment to bind other exogenous coligands. The test species were nitrate, nitrite, azide, hydrazine, pyrazolate (pz), pyridazine (pydz), phthalazine (phtz), and benzoate (OBz). These molecules are known to act as bridging ligands between metal ions,[31] and some of them are biologically important molecules. Herein we demonstrate that all species can be readily accommodated in the binding pocket of $[(L^{Me})Ni_2]^{2+}$. In each case we have obtained single crystals suitable for X-ray structure determinations. Therefore, it has been possible to study in detail the effect of the size and form of the binding pocket of the $[(L^{Me})Ni_2]^{2+}$ fragment on the coordination mode of the coligands and vice versa. The results of IR and UV/Vis spectroscopic investigations, cyclic voltammetry, binding studies, and variable-temperature magnetic susceptibility measurements are also reported.

Results and Discussion

Synthesis of complexes

Table 1 lists the synthesized complexes and their labels. Of these, the chloro- and acetato-bridged complexes **1** and **10** have been reported earlier. Scheme 2 depicts the synthetic procedures.

Table 1. Synthesized complexes and their labels.[a]

	$[(L^{Me})Ni_2(\mu\text{-}L')]^+$	L′
1[b]	$[(L^{Me})Ni_2(\mu\text{-}Cl)]^+$	chloride, Cl^-
2	$[(L^{Me})Ni_2(\mu\text{-}NO_3)]^+$	nitrate, NO_3^-
3	$[(L^{Me})Ni_2(\mu\text{-}NO_2)]^+$	nitrite, NO_2^-
4	$[(L^{Me})Ni_2(\mu\text{-}N_3)]^+$	azide, N_3^-
5	$[(L^{Me})Ni_2(\mu\text{-}N_2H_4)]^{2+}$	hydrazine, N_2H_4
6	$[(L^{Me})Ni_2(\mu\text{-}pz)]^+$	pyrazolate, $N_2C_3H_3^-$
7	$[(L^{Me})Ni_2(\mu\text{-}pydz)]^{2+}$	pyridazine, $N_2C_4H_4$
8	$[(L^{Me})Ni_2(\mu\text{-}phtz)]^{2+}$	phthalazine, $N_2C_8H_6$
9	$[(L^{Me})Ni_2(\mu\text{-}OBz)]^+$	benzoate, $C_6H_5CO_2^-$
10[c]	$[(L^{Me})Ni_2(\mu\text{-}OAc)]^+$	acetate, $CH_3CO_2^-$

[a] The complexes were isolated as ClO_4^- or BPh_4^- salts. [b] Ref. [28]. [c] Ref. [29].

Complexes **2**–**6** and **9** were synthesized by treatment of **1**-ClO_4 with a two- to fivefold excess of the sodium salt of the corresponding anion (or neat hydrazine hydrate in the case of **5**) in aqueous methanolic solution. In general, these reactions were complete within a few hours at ambient temperature and produced clear solutions from which, upon addition of an excess of $LiClO_4$, the yellow (**4**-ClO_4) or green per-

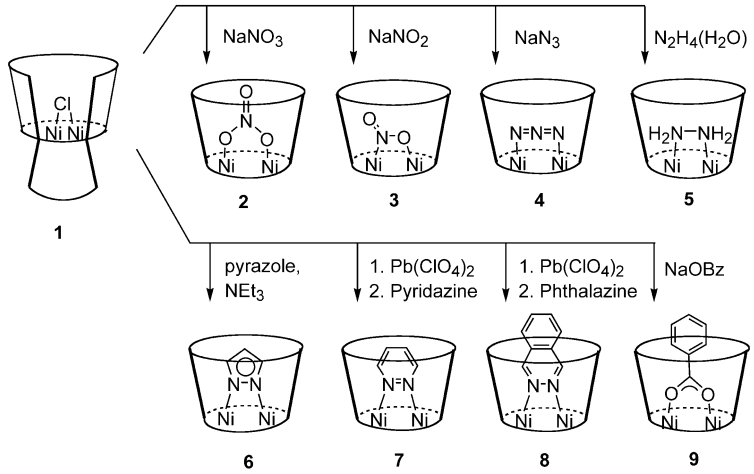

Scheme 2. Synthesis of compounds **2**–**9**. For ligand abbreviations see Scheme 1.

chlorate salts (**2**-ClO_4, **3**-ClO_4, **5**-$(ClO_4)_2$, **6**-ClO_4, and **9**-ClO_4) of the desired complexes precipitated as microcrystalline solids in good to excellent yields (73–89%). In two cases, **2**-NO_3 and **4**-N_3, the complexes were also obtained with the ligands (NO_3^- and N_3^-, respectively) as counteranions. The dicationic pyridazine and phthalazine derivatives **7** and **8** were prepared in acetonitrile solution, by treatment of **1** with lead perchlorate in acetonitrile, followed by removal of $PbCl_2$(s) by filtration and subsequent addition of the neutral diazine heterocycles. In this way, the diperchlorate salts **7**-$(ClO_4)_2$ and **8**-$(ClO_4)_2$ were obtained as brown crystals in similarly good yields. The monocations **3**, **4**, **6**, and **9** were also isolated as their tetraphenylborate salts.

All complexes are stable in air, both in solution and in the solid state. They exhibit good solubility in polar aprotic solvents such as acetonitrile, acetone, or dichloromethane. Both the perchlorate and the tetraphenylborate salts are not very soluble in alcohols and virtually insoluble in water. All compounds gave satisfactory elemental analyses and were characterized by spectroscopic methods, cyclic voltammetry, variable-temperature magnetic susceptibility measurements, and compounds **2**-$NO_3 \cdot H_2O \cdot$MeOH, **3**-$ClO_4 \cdot$MeOH, **4**-$N_3 \cdot 3$MeOH, **5**-$(ClO_4)_2$, **6**-$BPh_4 \cdot$MeCN, **7**-$(ClO_4)_2 \cdot 2$MeCN, **8**-$(ClO_4)_2 \cdot 0.5$EtOH, and **9**-BPh_4 also by X-ray structure analysis.

Characterization of the complexes

Infrared spectroscopy: Table 2 summarizes selected analytical data for the new compounds. In the infrared spectra of **2**–**9**, most of the stretching frequencies of the coligands are completely obscured by the absorptions of the $[(L^{Me})Ni_2^{II}]^{2+}$ fragment[32] and the counterions (ClO_4^- or BPh_4^-). Nevertheless some absorptions of the coligands could be detected. In the spectrum of **2**, for example, the bands at 1384 and 1277 cm^{-1} can be assigned to the asymmetric and symmetric stretching modes of a $\mu_{1,3}$-bridging nitrate ion.[33] Similarly, the band at 1183 cm^{-1} in the spectrum of **3** reveals the presence of a bridging NO_2^- group.[34] Likewise, in the spectrum of the azido complex **4** the strong band at 2059 cm^{-1} implicates a coordinated azide ion. The IR spectrum of hydrazine complex **5** shows sharp absorptions for the asymmetric and symmetric NH_2 stretching modes between 3300 and 3250 cm^{-1}, similar to other hydrazine complexes.[35,36] Unfortunately, for **6**–**8** no characteristic IR absorptions due to the coligands could be detected. Finally, in the spectrum of **9** the most prominent features are the intense bands at 1600 and 1427 cm^{-1}, which can be readily assigned to the asymmetric and symmetric carboxylate stretching modes.[37] The observed values are very similar to those of the acetato-bridged complex **10**, suggesting that the benzoate moiety in **9** is also in the $\mu_{1,3}$-bridging mode.

UV/Vis spectroscopy: The electronic absorption spectra of complexes **2**–**9** were recorded in the range 300–1600 nm in acetonitrile solution at ambient temperature. The spectra of the pale-green nickel complexes are similar but not identi-

Table 2. Selected infrared, UV/Vis, and electrochemical data for compounds **1**–**10**.

Cmpd	Band position [cm^{-1}]; assignment	λ_{max} [nm] (ε[M^{-1} cm^{-1}])[a]	E[V] (ΔE [V]) versus SCE[b]
1-ClO_4[c]		658 (41), 920 (59)	
		1002 (80)	
2-ClO_4	1384 + 1277; $\nu_{as} + \nu_s(\mu\text{-}NO_3^-)$	659 (46), 1049 (77)	0.71 (0.10), 1.51 (irr.)
3-ClO_4	1183; $\nu(\mu\text{-}NO_2^-)$	623 (39), 1104 (59)	0.74 (0.11), 1.44 (irr.)
3-BPh_4	1182; $\nu(\mu\text{-}NO_2^-)$	621 (40), 1111 (57)	
4-ClO_4	2059; $\nu(\mu\text{-}N_3^-)$	672 (37), 1092 (84)	0.58 (0.09), 1.53 (irr.)
4-BPh_4	2058; $\nu(\mu\text{-}N_3^-)$	673 (45), 1094 (102)	
4-N_3	2059; $\nu(\mu\text{-}N_3^-)$, 2036; $\nu(N_3^-)$		
5-$(ClO_4)_2$	3300, 3290, 3248; all ν(N–H)	624 (33), 1114 (67)	0.90 (0.11), 1.56 (irr.)
	1604; $\delta(NH_2)$, 952; ν(N–N)		
6-ClO_4		634 (24), 1178 (52)	0.58 (0.12), 1.24 (0.13)
6-BPh_4		634 (23), 1180 (52)	
7-$(ClO_4)_2$		615 (66), 1095 (62)	0.97 (irr)
8-$(ClO_4)_2$		629 (43), 1111 (57)	0.96 (irr)
9-ClO_4[d]	1600 + 1427; $\nu_{as} + \nu_s(\mu\text{-}CO_2)$	650 (30), 1118 (66)	0.51 (0.11), 1.28 (0.11)
9-BPh_4	1600 + 1427; $\nu_{as} + \nu_s(\mu\text{-}CO_2)$	650 (32), 1121 (67)	
		652 (38), 1118 (71)[e]	
10-ClO_4[f]	1588 + 1426; $\nu_{as} + \nu_s(\mu\text{-}CO_2)$	649 (28), 1134 (55)	0.56 (0.14), 1.36 (0.13)
10-BPh_4[f]	1585 + 1425; $\nu_{as} + \nu_s(\mu\text{-}CO_2)$	650 (29), 1135 (60)	

[a] Unless otherwise noted the spectra were recorded in CH_3CN solution at 295 K. Concentrations of solutions were $\sim 1.0 \times 10^{-3}$ M in sample. [b] Data recorded using the perchlorate salts in CH_3CN solution. All potentials are referenced to SCE. For experimental conditions see Experimental Section. $E = (E_p^{ox} + E_p^{red})/2$ for reversible one-electron transfer processes; values in parentheses represent peak-to-peak separations ($\Delta E_p = |E_p^{ox} - E_p^{red}|$). [c] Ref. [28]. [d] Ref. [38]. [e] Spectrum was recorded in CH_2Cl_2 solution at 295 K. [f] Ref. [29].

cal. Each compound displays two weak absorption bands. One appears in the 620 to 670 nm range, the other one is observed between 1050 and 1180 nm. These absorptions can be attributed to the d–d transitions ν_2 ($^3A_{2g}(F)\rightarrow{}^3T_{1g}(F)$) and ν_1 ($^3A_{2g}(F)\rightarrow{}^3T_{2g}(F)$), respectively, of an octahedral nickel(II) (d^8) ion. The higher energy features below 400 nm result from π–π* transitions within the $(L^{Me})^{2-}$ ligand. In summary, the slight differences in the position of the d–d transitions indicate that each complex retains its coligand in the solution state. This is also supported by the electrochemical properties described below.

Electrochemistry: All complexes were further characterized by cyclic voltammetry. Cyclic voltammograms have been recorded in CH_3CN solution with $[n\mathrm{Bu}_4\mathrm{N}]PF_6$ as the supporting electrolyte at a scan rate of 100 mV s^{-1}. Table 2 summarizes the electrochemical data. All potential values refer to the standard calomel electrode (SCE).

Figure 1 shows the cyclic voltammogram of the benzoato-bridged complex **9**.[38] This complex undergoes two reversible one-electron oxidations at very positive potentials, the

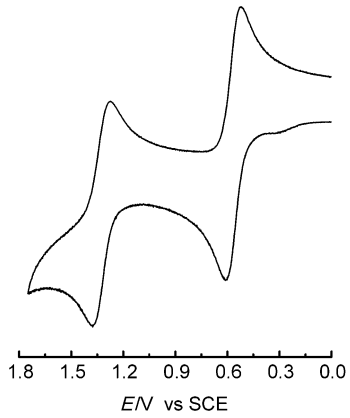

Figure 1. Cyclic voltammogram of $[(L^{Me})Ni_2(\mu\text{-}O_2CPh)]ClO_4$ (**9**-ClO_4) in CH_3CN (ca 1×10^{-3} M). Conditions: Pt working electrode, Pt wire auxiliary electrode, Ag wire reference electrode. 0.1 M $[(n\mathrm{Bu})_4\mathrm{N}]PF_6$ supporting electrolyte, scan rate 100 mV s^{-1}.

$E_{1/2}$ values being +0.51 ($\Delta E_p = 0.11$ V) and +1.28 V (0.11) versus SCE. The two processes are tentatively assigned to the formation of the mixed-valent $Ni^{II}Ni^{III}$ and $Ni^{III}Ni^{III}$ species,[39] as indicated in Equation (1).

$$[(L^{Me})Ni_2^{III}(\mu\text{-}L')]\underset{-e^-}{\overset{+e^-}{\rightleftharpoons}}[(L^{Me})Ni^{III}Ni^{II}(\mu\text{-}L')]^{2+}\underset{-e^-}{\overset{+e^-}{\rightleftharpoons}}[(L^{Me})Ni_2^{II}(\mu\text{-}L')]^{+} \quad (1)$$

The cyclic voltammograms of the other dinickel(II) complexes also reveal two redox waves with very positive oxidation potentials. However, the redox waves above about 0.90 V are all irreversible. Nevertheless, it can be clearly seen from Table 2 that the redox potentials of the $[(L^{Me})Ni_2^{II}(\mu\text{-}L')]^{n+}$ complexes depend on the coligand L′. The complexes **2**–**4**, **6**, and **9** with anionic coligands are all easier to oxidize (by ca. 0.40 V) than the complexes **5**, **7**, and **8** bearing neutral coligands. The lowering of the redox potentials in the former is presumably due to a stabilizing Coulomb attraction between the anionic coligands and the positively charged $[(L^{Me})Ni^{III}Ni^{II}]^{2+}$ species formed upon oxidation. The electrochemical data thus confirm the conclusions drawn from the UV/Vis spectroscopic studies that the $[(L^{Me})Ni_2(\mu\text{-}L')]^{n+}$ complexes retain their bioctahedral structures in the solution state.

X-ray crystallography: Although the formulations of the new compounds were reasonably substantiated by the above spectroscopic data, further confirmation was provided by X-ray diffraction studies. Single crystals of X-ray quality were obtained for all complexes in this series. All data collections were performed at 210 K. Selected crystallographic data are given in Table 3; see Supporting Information for complete listings.

The molecular structures of the complexes **2**–**9** are shown in Figures 2, S4 and S5 (for S4 and S5, see Supporting Information). A common labeling scheme for the $[(L^{Me})Ni_2]^{2+}$ segment (see Figure 3) has been used to facilitate structural

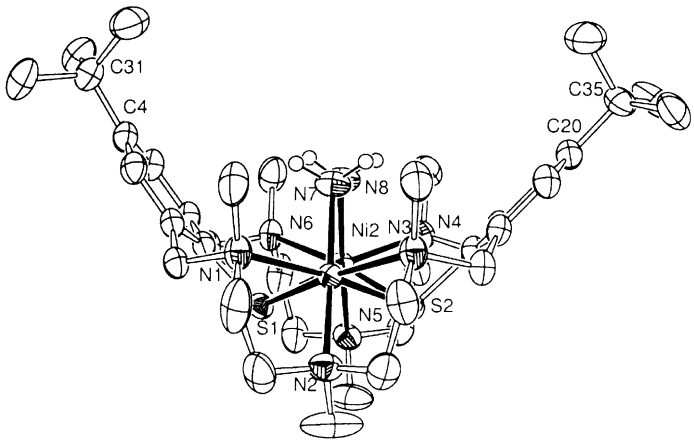

Figure 2. Molecular structure of the hydrazine complex **5**. Thermal ellipsoids are drawn at the 50% probability level. *tert*-butyl groups and hydrogen atoms are omitted for clarity. For the structures of the other complexes see Supporting Information.

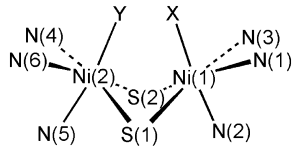

Figure 3. The common labeling scheme for the central $N_3Ni(\mu\text{-}S)_2NiN_3$ core of the $[(L^{Me})Ni_2]^{2+}$ fragment of complexes **2**–**10**.

comparisons. The structure of the cation $[(L^{Me})Ni_2^{II}(\mu\text{-}OAc)]^+$ (**10**) has been reported previously,[29] and its metrical parameters are also given for comparison. Selected bond lengths and angles are listed in Table 4 and Table 5, respectively.

Structure of the $[(L^{Me})Ni_2]^{2+}$ fragment: It is appropiate to discuss the structure of the $[(L^{Me})Ni_2]^{2+}$ subunit in **2**–**9** first.

Table 3. Selected crystallographic data for compounds **2–9**.

Compound	**2**-NO_3·H_2O·MeOH	**3**-ClO_4·MeOH	**4**-N_3·3 MeOH	**5**-$(ClO_4)_2$
formula	$C_{39}H_{69}N_8Ni_2O_8S_2$	$C_{39}H_{68}ClN_7Ni_2O_7S_2$	$C_{41}H_{76}N_{12}Ni_2O_3S_2$	$C_{38}H_{68}Cl_2N_8Ni_2O_8S_2$
M_r [g mol^{-1}]	959.56	963.99	966.68	1017.44
space group	$P\bar{1}$	$P\bar{1}$	$P\bar{1}$	$P\bar{1}$
a [Å]	13.187(5)	11.828(2)	12.887(3)	12.487(2)
b [Å]	13.860(5)	14.235(3)	14.039(3)	14.392(3)
c [Å]	14.240(5)	15.739(3)	14.216(3)	14.611(3)
α [°]	91.051(6)	102.94(3)	87.61(3)	101.23(3)
β [°]	105.359(6)	110.85(3)	73.44(3)	110.34(3)
γ [°]	94.851(6)	104.07(3)	87.20(3)	103.84(3)
V [Å^3]	2498.5(16)	2256.9(7)	2461.3(9)	2276.5(8)
Z	2	2	2	2
ρ_{calcd} [g cm^{-3}]	1.275	1.419	1.304	1.484
crystal size [mm^3]	0.15×0.15×0.15	0.30×0.20×0.20	0.15×0.20×0.30	0.30×0.30×0.30
μ($Mo_{K\alpha}$) [mm^{-1}]	0.890	1.040	0.898	1.094
2θ limits [°]	2.89–57.72	3.50–56.64	2.90–56.66	3.06–56.60
measured refl.	22337	20138	22638	20269
independent refl.	11610	10396	11595	10452
observed refl.[a]	6071	8036	5333	7898
no. parameters	509	520	515	541
$R1$[b] ($R1$ all data)	0.0791 (0.1421)	0.0358 (0.0478)	0.0435 (0.1240)	0.0339 (0.0498)
w$R2$[c] (w$R2$ all data)	0.2463 (0.2880)	0.1072 (0.1136)	0.0759 (0.0956)	0.0937 (0.1092)
max, min [e Å^{-3}]	2.906/−0.652	0.917/−0.547	0.506/−0.494	0.608/−0.525

Compound	**6**-BPh_4·MeCN	**7**-$(ClO_4)_2$·2 MeCN	**8**-$(ClO_4)_2$·0.5 EtOH	**9**-BPh_4
formula	$C_{67}H_{90}BN_9Ni_2S_2$	$C_{46}H_{74}Cl_2N_{10}Ni_2O_8S_2$	$C_{47}H_{73}Cl_2N_8Ni_2O_{8.50}S_2$	$C_{69}H_{89}BN_6Ni_2O_2S_2$
M_r [g mol^{-1}]	1213.83	1147.59	1138.57	1226.81
space group	$P\bar{1}$	$P2_1/n$	$P\bar{1}$	$P\bar{1}$
a [Å]	13.339(3)	14.697(3)	14.075(3)	15.752(3)
b [Å]	15.704(3)	25.044(5)	14.121(3)	15.926(3)
c [Å]	16.934(3)	15.827(3)	15.408(3)	27.275(5)
α [°]	108.643(3)	90	103.78(3)	103.02(3)
β [°]	92.132(3)	110.04(3)	101.34(3)	96.22(3)
γ [°]	107.876(3)	90	110.74(3)	105.18(3)
V [Å^3]	3162.7(10)	5473(2)	2645(1)	6331(2)
Z	2	4	2	4
ρ_{calcd} [g cm^{-3}]	1.275	1.393	1.458	1.287
crystal size [mm^3]	0.18×0.14×0.20	0.28×0.28×0.25	0.45×0.42×0.28	0.50×0.35×0.35
μ($Mo_{K\alpha}$) [mm^{-1}]	0.709	0.920	0.953	0.710
2θ limits [°]	2.90–57.80	3.18–56.58	3.26–56.74	2.74–56.68
measured refl.	28694	34004	23661	58022
independent refl.	14789	13033	12185	29801
observed refl.[a]	9032	8708	8248	11869
no. parameters	786	568	591	1533
$R1$[b] ($R1$ all data)	0.0463 (0.0875)	0.0326 (0.0590)	0.0470 (0.0755)	0.0422 (0.1454)
w$R2$[c] (w$R2$ all data)	0.0957 (0.1128)	0.0768 (0.0844)	0.1219 (0.1368)	0.0807 (0.1037)
max, min [e Å^{-3}]	0.679/−0.607	0.568/−0.337	0.892/−0.635	0.327/−0.554

[a] Observation criterion: $I > 2\sigma(I)$. [b] $R1 = \Sigma||F_o| - |F_c||/\Sigma|F_o|$. [c] $wR2 = \{(\Sigma[w(F_o^2 - F_c^2)^2]/\Sigma[w(F_o^2)^2]\}^{1/2}$.

In all eight new dinickel(II) complexes the macrocycle adopts the conical calixarene-like conformation previously reported for the acetato-bridged complex **10** (Form B, Scheme 1).[26,29] In this nearly C_{2v}-symmetric structure, the two nickel atoms are coordinated in a square-pyramidal fashion by the two *fac*-$N_3(\mu\text{-}S)_2$ donor sets of the doubly deprotonated macrocycle $(L^{Me})^{2-}$. Upon coordination of the exogenous coligands, distorted octahedral environments result for the two metal atoms. The structures of the dinuclear subunits are similar but not identical within the series. For example, the Ni···Ni distance varies from 3.392(1) to 3.683(1) Å. The metal–metal separations correlate with the nature of the bridging ligands. Complexes having multiple atom bridges such as $\mu_{1,3}$-carboxylate display longer Ni···Ni distances than complexes with $\mu_{1,2}$-bridges, such as NO_2^-. In addition, the respective metal–ligand bond lengths and angles of the $[(L^{Me})Ni_2]^{2+}$ unit also differ significantly from one structure to the other (see Table 4 and Table 5).

As in previously reported structures of this ligand system (e.g. $[(L^{Me})M_2(\mu\text{-OAc})]^+$, M = Co^{II}, Ni^{II}, and Zn^{II}),[26,29] the Ni–N bond lengths involving the four benzylic nitrogen donors are invariably longer (by ~0.1 Å) than the ones comprising the central nitrogen atoms of the linking diethylene triamine units. The short Ni–N2 and Ni–N5 bonds are therefore not a reflection of a *trans* influence of the coligand. Rather, the disparities in the metal–nitrogen bond lengths are almost certainly a consequence of the steric constraints of the macrocycle. The average bond lengths and angles, however, are in good agreement with those of other octahedral nickel(II) complexes with mixed thiophenolate/amine ligation.[40]

The dimensions of the bowl-shaped cavity of the $[(L^{Me})Ni_2]^{2+}$ fragment can be described by the intramolecular distance between the two opposing aryl ring carbon atoms C4 and C20 (see Figures 2, S4 and S5). Interestingly, this distance varies considerably across the present structures. The values range from 8.693 to 9.760 Å (Table 4). This implies secondary interactions between the guest molecules and the *N*-alkyl and *S*-4-*tert*-butylphenyl residues of the dinuclear $[(L^{Me})Ni_2]^{2+}$ subunit. Remarkably, the shortest distance occurs in the benzoato-bridged complex, in spite of the benzoate group being amongst the largest of the investigated guest molecules. For the smaller ionic ligands (NO_3^-, NO_2^-, N_3^-, OAc^-) the C4···C20 distance is in all cases longer by up to 1 Å. The distortions imposed by the benzoate moiety are indicative of attractive van der Waals interactions between the CH functions of the bowl-shaped host and its guest. As will be shown in more detail below, these secondary host–guest interactions play an important role as they confer unusual binding modes on the coligands.

Binding mode of the coligands: Figure 4 shows the binding modes of the coligands in compounds **2–10**, along with selected bond lengths and angles. As can be seen all coligands

Table 4. Selected bond lengths [Å] in **2**–**10**.

Complex[a] X, Y[c]	**2**, NO_3^- O1, O2	**3**, NO_2^- N7, O1	**4**, N_3^- N9, N7	**5**, N_2H_4 N7, N8	**6**, pyraz N8, N7	**7**, pydz N7, N8	**8**, phtz N7, N8	**9**, OBz[b] O1A,B; O2A,B	**10**, OAc[f] O1, O2
Ni1–X[c]	2.058(4)	2.141(2)	2.102(3)	2.092(2)	2.044(2)	2.117(2)	2.135(3)	2.007(2) [1.995(2)]	1.998(2)
Ni1–N1	2.276(5)	2.295(2)	2.200(3)	2.268(2)	2.337(2)	2.343(2)	2.395(3)	2.322(3) [2.207(3)]	2.281(2)
Ni1–N2	2.138(5)	2.167(2)	2.136(3)	2.114(2)	2.179(2)	2.132(2)	2.134(3)	2.137(3) [2.123(3)]	2.152(2)
Ni1–N3	2.231(5)	2.245(2)	2.226(3)	2.269(2)	2.272(2)	2.281(2)	2.237(3)	2.197(3) [2.342(3)]	2.251(2)
Ni1–S1	2.464(2)	2.475(1)	2.520(1)	2.503(1)	2.500(1)	2.453(1)	2.469(0)	2.452(1) [2.493(2)]	2.493(1)
Ni1–S2	2.444(2)	2.463(1)	2.507(1)	2.477(1)	2.450(1)	2.450(1)	2.432(1)	2.509(2) [2.452(1)]	2.448(1)
Ni2–Y[c]	2.083(4)	2.081(2)	2.095(3)	2.142(2)	2.038(2)	2.138(2)	2.108(3)	2.004(2) [2.013(2)]	2.008(2)
Ni2–N4	2.212(5)	2.321(2)	2.212(3)	2.268(2)	2.270(2)	2.338(2)	2.253(3)	2.274(3) [2.202(3)]	2.244(2)
Ni2–N5	2.137(5)	2.140(2)	2.135(3)	2.140(2)	2.178(2)	2.126(2)	2.150(2)	2.133(3) [2.166(3)]	2.158(2)
Ni2–N6	2.297(5)	2.236(2)	2.248(3)	2.284(2)	2.342(2)	2.268(2)	2.382(2)	2.259(3) [2.338(3)]	2.295(2)
Ni2–S1	2.4705(19)	2.475(1)	2.510(1)	2.478(1)	2.499(1)	2.450(1)	2.476(1)	2.506(2) [2.441(1)]	2.493(1)
Ni2–S2	2.4372(18)	2.457(1)	2.494(1)	2.473(1)	2.455(1)	2.451(1)	2.415(1)	2.445(1) [2.485(1)]	2.451(1)
M–N[d]	2.215(5)	2.234(2)	2.193(3)	2.224(2)	2.263(2)	2.248(2)	2.259(3)	2.220(3) [2.230(3)]	2.230(2)
M–S[d]	2.454(2)	2.467(1)	2.507(1)	2.482(1)	2.476(1)	2.451(1)	2.448(2)	2.478(1) [2.468(1)]	2.471(1)
Ni···Ni	3.492(2)	3.398(1)	3.683(1)	3.441(1)	3.389(1)	3.392(1)	3.402(1)	3.491(1) [3.448(1)]	3.483(1)
C4···C20[e]	9.712	9.349	9.419	9.367	9.395	8.955	9.760	8.693 [8.948]	9.306

[a] Complex names are abbreviated to the exogenous ligands for clarity. [b] There are two crystallographically independent molecules A and B in the unit cell. Values in square brackets refer to molecule B. [c] X and Y denote the donor atoms of the coligands. [d] Mean values. [e] Distance between the two aromatic carbons bearing the *tert*-butyl groups. [f] Ref. [28].

Table 5. Selected angles [°] in **2**–**10**.

Complex X, Y[b]	**2**, NO_3^- O1, O2	**3**, NO_2^- N7, O1	**4**, N_3^- N9, N7	**5**, N_2H_4 N7, N8	**6**, pz N8, N7	**7**, pydz N7, N8	**8**, phtz N7, N8	**9**, OBz[a] O1A,B, O2A,B	**10**, OAc O1,O2
X-Ni1-N2[b]	163.5(2)	175.89(8)	165.78(11)	172.90(8)	175.31(9)	176.98(6)	175.02(10)	164.57(11) [165.11(11)]	163.89(7)
N3-Ni1-S1	169.47(14)	172.18(5)	166.56(7)	170.04(5)	170.61(6)	172.30(5)	171.01(7)	171.06(8) [169.79(8)]	170.09(5)
N1-Ni1-S2	169.82(14)	170.39(6)	167.09(8)	170.99(6)	169.58(6)	170.59(4)	168.53(7)	170.46(8) [171.01(8)]	170.28(5)
X-Ni1-S1	92.30(13)	84.13(6)	92.82(9)	86.76(7)	86.72(6)	85.78(4)	84.75(7)	91.05(7) [97.38(8)]	93.30(5)
X-Ni1-S2	94.55(14)	85.48(6)	91.86(9)	87.69(7)	88.27(6)	87.17(5)	89.00(8)	96.38(8) [91.49(8)]	94.78(6)
X-Ni1-N1	86.8(2)	97.71(8)	87.54(11)	93.44(9)	96.58(8)	96.56(6)	95.99(10)	87.01(10) [87.94(10)]	87.69(8)
X-Ni1-N3	87.6(2)	94.95(8)	88.37(11)	93.33(9)	95.72(9)	94.88(6)	95.73(10)	88.62(10) [87.44(10)]	87.77(8)
N1-Ni1-N3	99.69(19)	97.91(8)	101.63(10)	99.28(8)	98.54(8)	97.49(6)	99.21(9)	97.49(11) [98.36(11)]	98.90(8)
S1-Ni1-S2	79.06(6)	81.38(4)	75.35(4)	80.48(4)	80.89(3)	81.58(2)	80.50(3)	79.64(4) [80.34(4)]	79.49(4)
Y-Ni2-N5	163.4(2)	171.91(7)	166.17(11)	173.53(8)	175.22(8)	177.98(7)	174.19(10)	165.31(12) [164.54(11)]	163.84(7)
N4-Ni2-S1	170.24(14)	170.28(5)	167.31(7)	171.16(6)	171.39(6)	171.05(5)	171.42(6)	170.10(9) [171.39(8)]	170.86(5)
N6-Ni2-S2	169.06(15)	172.99(5)	166.48(7)	170.89(6)	168.95(6)	172.44(4)	168.93(7)	171.33(9) [169.29(8)]	169.28(5)
Y-Ni2-S1	91.60(14)	87.78(5)	91.38(8)	87.32(7)	87.01(6)	87.09(5)	85.93(7)	95.20(8) [91.65(7)]	93.55(6)
Y-Ni2-S2	95.28(14)	86.70(5)	93.79(9)	86.09(7)	87.92(6)	85.69(5)	88.39(8)	93.35(7) [97.60(8)]	95.44(5)
Y-Ni2-N4	87.7(2)	94.43(7)	88.72(11)	92.89(9)	95.92(8)	96.78(7)	95.75(10)	88.15(11) [88.20(10)]	87.79(8)
Y-Ni2-N6	86.3(2)	92.02(8)	87.36(11)	95.39(9)	96.57(8)	96.01(6)	94.37(10)	87.49(11) [88.72(11)]	88.11(7)
N4-Ni2-N6	99.61(19)	97.82(8)	101.93(10)	98.74(8)	98.33(8)	96.50(6)	99.41(9)	97.97(12) [98.11(11)]	98.83(7)
S1-Ni2-S2	79.07(6)	81.51(4)	75.76(4)	81.05(5)	80.78(3)	81.62(2)	80.67(4)	79.83(4) [80.73(4)]	79.45(3)
Ni1-S1-Ni2	90.10(6)	86.69(3)	94.20(4)	87.40(4)	85.35(3)	87.55(2)	86.95(4)	89.51(4) [88.65(4)]	88.63(4)
Ni1-S2-Ni2	91.36(6)	87.37(5)	94.90(4)	88.09(5)	87.40(3)	87.61(3)	89.18(4)	89.60(4) [88.58(4)]	90.66(3)
Ph/Ph[c]	88.3(2)	80.3(2)	85.0(2)	80.0(2)	81.8(2)	72.9(2)	88.7(2)	67.4(2) [72.5]	80.8(2)

[a] There are two crystallographically independent molecules A and B in the unit cell. Values in square brackets refer to molecule B. [b] X and Y denote the donor atoms of the coligands. [c] Angle between the normals of the planes of the aryl rings.

act as bidentate $\mu_{1,n}$-bridges ($n=2$ or 3). Apparently, in $[(L^{Me})Ni_2(\mu\text{-}L')]$ complexes of structure type B L′ cannot be a *single*-atom ($\mu_{1,1}$)-bridging ligand. This seems to be possible only for complexes of the alternative structure type A. In other words, multi-atom bridging ligands induce the $[(L^{Me})Ni_2]^{2+}$ fragment to adopt a structure of the kind B, whereas single-atom bridges such as Cl^- or OH^- support the conformation of type A. It is also worth mentioning, that the hexazadithiophenolate ligand supports triply bridged $N_3M(\mu\text{-}SR)_2(\mu\text{-}L')MN_3$ core structures at all. Martell and coworkers, for example, have recently investigated the ligating properties of the analogous hexaazadiphenolate ligand systems. Despite the identical ligand backbones, only doubly bridged $N_3M(\mu\text{-}OR)_2MN_3$ core structures are supported.[41] It can be assumed that these differences are a result of the different hybridizations of the phenolate-oxygen (sp^2, trigonal-planar) and the thiophenolate-sulfur atoms (sp^3, tetrahedral). The former macrocycles tend to enforce a planar $M(\mu\text{-}OR)_2M$ core, while the latter feature a bent $M_2(\mu\text{-}SR)_2$ ring, which can be spanned better by the exogenous ligands.

In the following the binding modes of the coligands are described in detail. As can be seen in Figure 4, the nitrate ion in **2** is coordinated in a symmetrical $\mu_{1,3}$-fashion. This is a typical coordination mode of this anion,[42] and it has been observed previously in other nitrato-bridged complexes.[43,44] The average Ni–O bond length (2.071(4) Å) is significantly longer than in the $\mu_{1,3}$-carboxylato-bridged species **9** and **10**, implying that the Ni–nitrate bonds are weaker than the Ni–

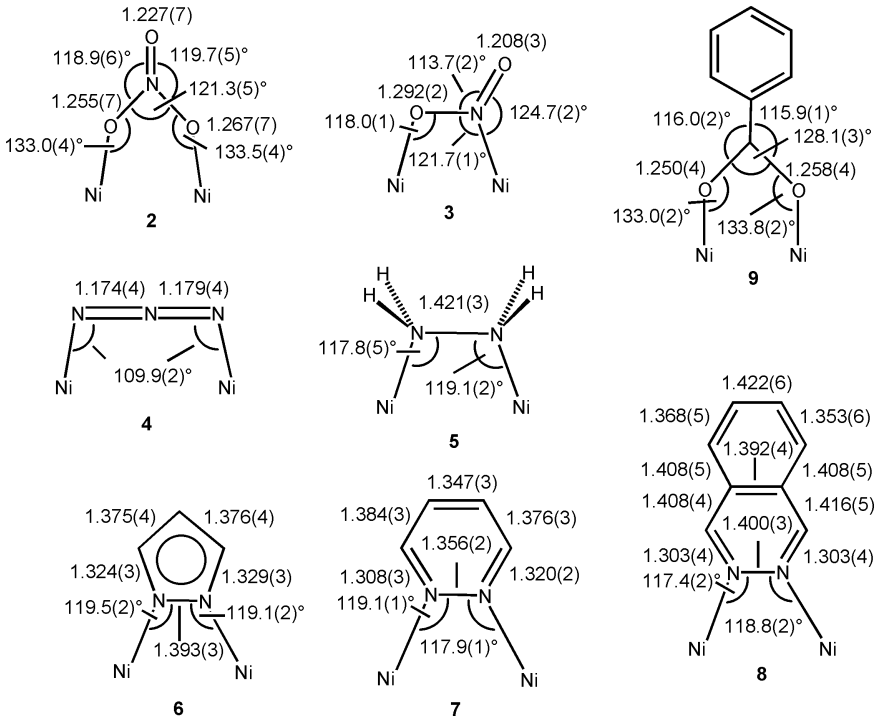

Figure 4. Binding mode, bond lengths [Å], and angles [°] of the coligands in **2**–**9**.

carboxylate bonds. This nicely corroborates with the results of the binding studies presented below, which reveal that the nitrate group is readily replaced by carboxylate anions, but not vice versa. The planar NO_3^- group aligns almost parallel with an adjacent phenyl ring. It is 3.30 to 3.44 Å from the mean plane of this phenyl ring. This is indicative of an intramolecular π–π stacking interaction.[45]

The nitrite ion can bridge two metal ions in several ways.[31,46–48] In the present case, the $\mu_{1,2}$- (N,O-bound NO_2^-) and the $\mu_{1,3}$-modes (O,O-bound NO_2^-) are of relevance. The symmetrical $\mu_{1,3}$-binding motif seems to be geometrically feasible in view of the observed $\mu_{1,3}$-nitrate function in **2**, but the crystal structure reveals the bridging $\mu_{1,2}$-*nitro*-form. This is presumably due to a more "relaxed" structure of the $[(L^{Me})Ni_2]^{2+}$ fragment in the latter mode of coordination. This is also supported by the fact that the octahedral Ni centers in **3** are much less distorted than in **2**.

A large number of dinuclear nickel complexes with azide linkages exist in the literature.[49–51] This linear triatomic anion can join two Ni centers in an end-on ($\mu_{1,1}$-N_3) or an end-to-end motif ($\mu_{1,3}$-N_3). The latter is seen in the present structure. Of note are the Ni-N-N angles of 109.9(2)° (which are remarkably obtuse for a $\mu_{1,3}$-bridging azide ion) in combination with the planarity of the Ni-N_3-Ni assembly (torsional angle $\tau = 0°$). This clearly shows that the binding pocket of the $[(L^{Me})Ni_2]^{2+}$ complex allows for the accommodation of anionic guest molecules in unusual coordination modes. A similar effect has been observed by McKee and Nelson. They were able to stabilize a nearly linear Ni-($\mu_{1,3}$-N_3)-Ni linkage in the cavity of a dinuclear nickel cryptate complex.[52] The magnetic properties of nickel complexes with such extreme azide coordination modes are of interest, because the theory predicts unusual large intramolecular magnetic exchange interactions for these species (see below).[53]

The hydrazine complex **5** provides an example for an unusual conformation of a small inorganic molecule. It is known that free hydrazine exists predominantly in the *gauche* conformation at room temperature (dihedral angle $\tau \sim 100°$).[54] This conformation is also most commonly seen in dinuclear hydrazine complexes.[55] In the present complex the N_2H_4 ligand can only adopt the *cis* (ecliptic) conformation ($\tau = 3.7°$). To the best of our knowlege, such a coordination mode is without precedence in dinuclear transition-metal hydrazine complexes,[56,57] albeit it is documented for mononuclear species.[58] The hydrazine has a N7–N8 bond length of 1.421(3) Å consistent with a N–N single bond. A perchlorate ion is located above the N_2H_4 molecule, between the two *tert*-butyl groups (see Figure S1, Supporting Information). Three of its oxygen atoms form weak hydrogen bonds with the N_2H_4 hydrogen atoms (average NH···O and N···O distances 2.370 and 2.914 Å), but on the basis of similar long NH···C distances to some of the adjacent aryl carbon atoms (i.e. C2, C6, C16, C18; average value 2.968 Å), the presence of repulsive NH···C_{aryl} van der Waals interactions cannot be excluded. The observed ecliptic N_2H_4 conformation would not argue against such an intramolecular steric interaction. It should also be remembered that NH_4^+ ions can form hydrogen bonds with the π-electrons of phenyl rings.[59]

As expected, pyrazolate, pyridazine and phthalazine[60] bind to the $[(L^{Me})Ni_2]^{2+}$ fragment as bidendate bridges through their two ring nitrogens. Consequently, the Ni···Ni distances are nearly identical in these three compounds (average value is 3.394(1) Å). The average Ni–N(heterocycle) bond lengths to the pyrazolate moiety at 2.041 Å are shorter than to the pyridazine (2.128 Å) and phthalazine hetrocycles (2.122 Å), indicating that the pyrazolate anion interacts more strongly with the $[(L^{Me})Ni_2]^{2+}$ subunit than the two neutral diazine molecules. This is further supported by the ligand exchange reactions (see below), which reveal that $[(L^{Me})Ni_2]^{2+}$ binds the pyrazolate anion preferentially over the neutral diazines. The C–N and N–N distances of the η^2-bound heterocycles do not deviate significantly from the distances found in the free heterocycles alone[61] or in other dinuclear nickel(II) complexes of these N-heterocyclic ligand systems.[62] Unlike the pyrazolate and the pyridazine, the phthalazine moiety is tilted out of the Ni1-N7-N8-Ni2 plane towards one of the *tert*-butyl groups, presumably again as a result of hydrophobic interactions between the adjacent CH groups of the phthalazine moiety and the *tert*-butyl methyl

groups. The pyrazolate and pyridazine structures strongly support these assumptions. These heterocycles are smaller than the phthalazine ring and cannot experience these interactions, because they are too far away from the *tert*-butyl groups. In **8**, there is also an intermolecular π–π interaction that occurs between the exposed phthalazine faces of two opposing complexes (Figure S2, Supporting Information).

Last but not least, the benzoate ion in **9** chelates the two Ni^{II} ions in a symmetrical $\mu_{1,3}$-fashion, as was previously observed for the acetate group in **10** and already indicated by the IR data. The benzoate phenyl ring is twisted slightly out of the Ni1-O1-C39-O2-Ni2 mean plane such that relatively short contacts between the aryl-hydrogen atoms H44a,b, H42a,b and the hydrogen atoms of the *tert*-butyl methyl groups (2.397–3.236 Å) result. The structure is otherwise identical with that of **10**.

Exchange experiments: We have carried out a series of simple exchange experiments to estimate the relative binding affinities of the coligands. Each reaction was conducted at ambient temperature in a mixed acetonitrile/ethanol (1:1) solvent system using a tenfold excess of the coligand L″, according to Equation (2).

$$[(L^{Me})Ni_2(\mu\text{-}L')]^{n+} + L'' \rightleftharpoons [(L^{Me})Ni_2(\mu\text{-}L'')]^{n+} + L' \qquad (2)$$

The reactions were terminated after 5 h (the time after which no more changes occurred) and the solid products examined by IR spectroscopy.[63] If the IR spectrum of the isolated solid matched more closely with that of the starting material, $[(L^{Me})Ni_2(\mu\text{-}L')]^{n+}$, the binding affinity of the coligand L″ was estimated to be less than that of L′. In the other case, L″ was termed a stronger ligand than L′. This was ascertained by successive control experiments, in which the same reactions were run in the reverse direction, but now with L′ in tenfold excess over $[(L^{Me})Ni_2(\mu\text{-}L'')]^{n+}$.[64] In this way the relative binding affinities were determined as follows: pyridazine (**7**) ~ phthalazine (**8**) < nitrate (**2**) < hydrazine (**5**) < nitrite (**3**) < pyrazolate (**6**) < azide (**4**) < acetate (**10**) < benzoate (**9**).

Two trends are apparent. First, the $[(L^{Me})Ni_2]^{2+}$ complex binds anionic ligands preferentially over neutral species. This can be readily explained by the Coulomb attraction between the positively charged $[(L^{Me})Ni_2]^{2+}$ subunit and the negatively charged coligands. Second, the binding affinity of the anions parallels their position in the spectrochemical series.[65] This suggests that strong-field ligands are preferentially bound over weak-field ligands. It is, however, surprising that the benzoate group binds more strongly than the acetate group, in spite of the fact that the acetate is a stronger ligand.[66] We assume that these differences are due to hydrophobic effects,[67] as was already indicated by the crystal structure of **9**. This shows that the secondary host–guest interactions also contribute to the stability of the complexes.

Magnetic susceptibility measurements: The magnetic properties of complexes **3**-BPh_4, **4**-BPh_4, **7**-ClO_4, **9**-BPh_4, and **10**-BPh_4 were examined between 2.0 and 300 K by using a SQUID magnetometer in an applied external magnetic field of 0.2 T. The data are displayed in Figure 5 in the form of $\chi_M T$ versus T plots (for **10**-BPh_4, see Figure S3 Supporting Information).

For complex **3**-BPh_4 the product $\chi_M T$ gradually increases from 2.54 $cm^3 K mol^{-1}$ at 300 K (4.51 μ_B per dinuclear complex) to a maximum of 3.14 $cm^3 K mol^{-1}$ (5.01 μ_B) at 22 K, and then decreases rapidly to 2.56 $cm^3 K mol^{-1}$ at 2 K. This behavior indicates an intramolecular ferromagnetic exchange interaction between the two Ni^{II} ions in **3**. The abrupt decrease in $\chi_M T$ below 22 K is presumably due to zero-field splitting of Ni^{II}. A similar behavior is observed for the complexes **7**, **9**, and **10**, implicating that the coupling between the Ni^{II} ions in these three complexes is also ferromagnetic in nature. Therefore, the nitrito, pyridazine, and the carboxylato-bridged nickel complexes all exhibit an $S = 2$ spin ground state.

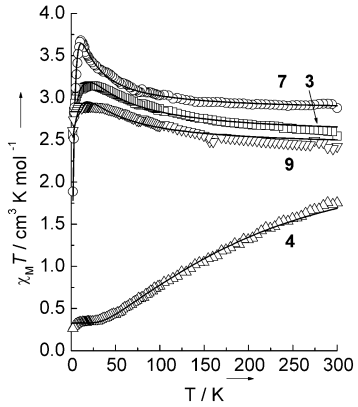

Figure 5. Plots of $\chi_m T$ against T for **3**-BPh_4 (□), **4**-BPh_4 (△), **7**-$(ClO_4)_2$ (○), and **9**-BPh_4 (▽). The full lines represent the best theoretical fits to the spin-Hamiltonian [Eq. (3)] (or [Eq. (4)] in the case of **4**). The fit parameters are summarized in Table 6. The experimental and calculated susceptibility values are provided in the Supporting Information.

The cryomagnetic behavior of the azido-bridged complex **4**-BPh_4 is completely different. In this case the value of $\chi_M T$, 1.75 $cm^3 K mol^{-1}$ at 300 K (3.74 μ_B per dinuclear complex), first decreases monotonically until it reaches a plateau at ~40 K of 0.39 $cm^3 K mol^{-1}$ (1.77 μ_B), and then decreases slowly to 0.26 $cm^3 K mol^{-1}$ (1.44 μ_B) at 2 K. The decrease of the $\chi_M T$ values at lower temperatures (40–2 K) is presumably due to the presence of a paramagnetic impurity.[68] Nevertheless, the overall behavior indicates an antiferromagnetic coupling between the two nickel(II) ions in complex **4**. Thus, complex **4** possesses a diamagnetic $S = 0$ ground state. This clearly shows that the spin ground state of the $[(L^{Me})Ni_2(\mu\text{-}L')]^{n+}$ fragment depends on the type of the coligand L′.

To determine the magnitude of the exchange interaction the $\chi_M T$ versus T experimental data were analyzed by using the isotropic Heisenberg–Dirac–van-Vleck (HDvV) exchange Hamiltonian [Eq. (3)] for dinuclear complexes,[69] which includes two additional terms to account for Zeeman splitting and single-ion zero-field interactions. The introduction of a D parameter is appropiate since for nickel(II) ions, the non-cubic components of the ligand field may act on the

$S=1$ ground state to produce a zero-field splitting which may be of the same order of magnitude as J.[70,71]

$$\boldsymbol{H} = -2J\mathbf{S}_1\mathbf{S}_2 + \sum_{i=1}^{2}\left\{D_i(S_{iz}^2 - \frac{1}{3}S_i(S_i+1)) + g_i\mu_B B S_i\right\} \qquad (3)$$

To reduce the number of the variables the D and g values were considered to be identical for the two nickel(II) ions. The resulting Hamiltonian was diagonalized numerically to obtain the magnetic susceptibility which was used to fit the $\chi_M T$ magnetic data for the nickel(II) compounds. The solid lines in Figure 5 represent the best fits. Table 6 contains the

Table 6. Magnetic properties of complexes **3**, **4**, **7**, **9**, and **10**.[a]

Complex	J [cm^{-1}]	g	D [cm^{-1}]
3 [(L^{Me})Ni$_2$(μ-NO$_2$)]BPh$_4$	+6.7	2.26	−32.2
4 [(L^{Me})Ni$_2$(μ-N$_3$)]BPh$_4$	−45.6	2.25(fixed)	0.0 (fixed)
	−58.9[b]	2.25[b]	
7 [(L^{Me})Ni$_2$(μ-pydz)](ClO$_4$)$_2$	+3.5	2.38	+9.53
9 [(L^{Me})Ni$_2$(μ-OBz)]BPh$_4$	+5.8	2.20	−32.0
10 [(L^{Me})Ni$_2$(μ-OAc)]BPh$_4$	+7.9	2.21(fixed)	−37.7

[a] Parameters resultant from least-squares fit to the $\chi_M T$ data under the spin Hamiltonian in [Eq. (3)], J=coupling constant ($\boldsymbol{H}=-2J\mathbf{S}_1\mathbf{S}_2$), g=g-value, D=zero-field-splitting parameter. [b] Parameters resultant from least-squares fit of the $\chi_M T$ data to the expression in [Eq. (4)].

corresponding fit parameters. The J values lie between +3.5 and +7.9 cm^{-1}, while the g values are in range 2.20–2.38. In all cases, the inclusion of the D parameter improved the low-temperature fit significantly, but they represent by no means an accurate value (temperature-dependent magnetic susceptibility measurement are not very appropriate for the determination of the sign and magnitude of D).[72,73]

In the case of complex **4**, a fit of the experimental data over the full temperature range was only possible to the theoretical expression in Equation (4) derived from the simple spin Hamiltonian $\boldsymbol{H}=-2J\mathbf{S}_1\mathbf{S}_2$ ($S_1=S_2=1$) by considering a fraction ρ of a paramagnetic impurity.[74,75]

$$\chi = \chi_{dim}(1-\rho) + 2\chi_{mono}\rho \qquad (4)$$

A least-squares fit of Equation (4) to the data yielded $J=-58.9$ cm^{-1} and $g=2.25$, while ρ was found to be 12%. We also tried to fit the data to the more explicit expression in Equation (3) by considering only the high-temperature (50–300 K) data. A fit was possible, but with the J value being the only variable. The D and g values had to be fixed ($D=0$ cm^{-1}, $g=2.25$) to produce a stable fit and the paramagnetic impurity had to be neglected. From this fit the J value was established to be −45.6 cm^{-1}, albeit the experimental $\chi_M T$ data could not be reproduced in every detail. Thus, the large amount of the paramagnetic impurity prevented the determination of an accurate J value for compound **4**. At the moment it can only be estimated to lie somewhere between −45 and −60 cm^{-1}.

The ferromagnetic exchange interaction in complexes **3**, **7**, **9**, and **10** can be rationalized in terms of the Goodenough–Kanamori rules for superexchange.[76] It can be assumed that the magnetic exchange interactions are predominantly transmitted via the thiophenolate-sulfur-atom pathway. This is not unreasonable given that the J values for the above four complexes do not vary much with variation of the coligand L′. The ferromagnetic coupling through the thiophenolate-sulfur-atom pathway remains to be explained, but this is straightforward:[77] For face-sharing bioctahedral nickel complexes a ferromagnetic exchange interaction is predicted if the Ni-X-Ni bridging angle is at 90°. For smaller angles, the orthogonality of the magnetic orbitals is cancelled and antiferromagnetic pathways become available to produce a change of the sign of J. An antiferromagnetic exchange interaction, for example, is observed in tris(μ-chloro)- or tris(μ-thiophenolato)-bridged complexes, where the average bridging angle is below 80°.[78] The other extreme is represented by the tris(μ-phenolato)-bridged complexes, which feature wider angles at 90±8° and hence parallel spin alignment occurs.[79] In our case, the Ni-(μ-SR)-Ni angles are very close to 90°, and hence in the range where the ferromagnetic pathway is the preferred one.

For **4**, the antiferromagnetic coupling between the two Ni^{II} ($S=1$) ions can be explained by assuming a strong antiferromagnetic exchange interaction through the azide ion which overcomes the ferromagnetic coupling through the thiolate bridges. This is supported by the fact that nearly all $\mu_{1,3}$-azido-bridged Ni^{II} ions feature an antiferromagnetic exchange interaction.[80] Moreover, it has recently been demonstrated that the sign and magnitude of the exchange interaction in $\mu_{1,3}$-azido-bridged nickel complexes depend on the Ni-N–N bond angles and the Ni-N$_3$-Ni torsional angles.[53,81] The largest antiferromagnetic exchange interaction is expected for a Ni-N-N bond angle of 108° and a torsional angle $\tau=0$°. Our observation of a strong antiferromagnetic exchange interaction in **4** in which the azide features exactly these metrical parameters is in good agreement with the reported trend.

Conclusion

In the present study the capability of the [(L^{Me})Ni$_2$]$^{2+}$ complex to bind a range of coligands other than chloride, hydroxide, and acetate has been demonstrated. The structural characterization of eight new complexes bearing anionic (NO$_3^-$, NO$_2^-$, N$_3^-$, pyrazolate, benzoate) and neutral coligands (hydrazine, pyridazine, phthalazine) shows that in each case only one of several possible coordination modes is realized. The presence of these distinct binding motifs can be traced back to the complementary size and form of the binding pocket of the [(L^{Me})Ni$_2$]$^{2+}$ fragment. In some cases, the binding pocket confers very unusual coordination modes ($\mu_{1,3}$-N$_3$) or conformations (ecliptic N$_2$H$_4$) on the coligands. In other instances, intramolecular host–guest interactions are present. Most importantly, the exogenous substrate influences many properties of the dinuclear complex fragment, including complex stability, redox potential, and ground spin-state. Since the complex integrity is retained in the solution state, the reactivity of these compounds can now also be examined.

Experimental Section

Materials: Unless otherwise noted the preparations of the metal complexes were carried out under an argon atmosphere by using standard Schlenk techniques. The compounds $H_2L^{Me}\cdot 6HCl$, $[(L^{Me})Ni_2(\mu\text{-}Cl)]ClO_4$ (**1**-ClO_4) and $[(L^{Me})Ni_2(\mu\text{-}OAc)]BPh_4$ (**10**-BPh_4) were prepared as described in the literature.[26]

Caution: *Perchlorate salts of transition metal complexes are hazardous and may explode. Only small quantities should be prepared and great care taken. The same is true for azide salts.*

$[(L^{Me})Ni_2(\mu\text{-}NO_3)]ClO_4$ (2-ClO_4): A solution of $NaNO_3$ (85 mg, 1.0 mmol) in H_2O (1.5 mL) was added to a solution of **1**-ClO_4 (184 mg, 0.20 mmol) in methanol (40 mL). The mixture was stirred for 4 h, during which time the color of the reaction mixture turned from yellow to green. Solid $LiClO_4\cdot 3H_2O$ (320 mg, 2.00 mmol) was added. The solution was stirred for a further 2 h during which time a pale-green solid precipitated. This solid was isolated by filtration, washed with little cold methanol, and recrystallized from a mixed acetonitrile/ethanol (1:1) solution to give pale-green crystals of the title compound. Yield: 152 mg (83%); m.p. 324–325°C (decomp); IR (KBr): $\tilde{\nu}$=2962s, 2953sh, 2899s, 2867s, 2811m, 1490m, 1456s, 1436sh, 1394m, 1384m [$\nu_{as}(NO_3^-)$], 1363m, 1345w, 1325w, 1308w, 1291w, 1277 [$\nu_s(NO_3^-)$], 1264m, 1234s, 1201 m, 1171w, 1152w, 1095vs [$\nu(ClO_4^-)$], 1056s, 1038w, 1001w, 982w, 931m, 912m, 882m, 826m, 818m, 808m, 753w, 743vw, 695w, 668w, 630sh, 623s, 601w, 565m, 544w, 535w, 492w, 470, 440w, 418w, 415w cm^{-1}; UV/Vis (CH_3OH): λ_{max} (ε)=659(46), 1049 (77) nm ($M^{-1}cm^{-1}$); CV(CH_3CN, 295 K, 0.1 M nBu_4NPF_6, ν=100 mV s^{-1}; E(V) vs SCE): $E^1_{1/2}$=+ 0.71 (ΔE_p 103 mV), E^2_{pa}=+ 1.51 (irr.); elemental analysis calcd (%) for $C_{38}H_{64}ClN_7Ni_2O_7S_2\,H_2O$ (965.94): C 47.25, H 6.89, N 10.15, S 6.64; found: C 47.27, H 6.96, N 10.07, S 6.74.

$[(L^{Me})Ni_2(\mu\text{-}NO_3)]NO_3$ (2-NO_3): A solution of $NaNO_3$ (85 mg, 1.0 mmol) in water (1.5 mL) was added to a solution of **1**-ClO_4 (184 mg, 0.20 mmol) in methanol (40 mL). The mixture was stirred for 4 h, during which time the color of the reaction mixture turned from yellow to green. The mixture was filtered and left to stand for two days at room temperature during which time green blocks of the title compound precipitated. This material was filtered, washed with methanol (1 mL) and dried in air. Yield: 145 mg (80%); m.p. >300°C (decomp); IR (KBr): $\tilde{\nu}$= 1384 [$\nu_{as}(NO_3^-)$], 1277 cm^{-1} [$\nu_s(NO_3^-)$]; elemental analysis calcd (%) for $C_{38}H_{64}N_8Ni_2O_6S_2$ (910.48): C 50.13, H 7.09, N 12.31, S 7.04; found: C 49.87, H 7.04, N 12.17, S 6.85.

$[(L^{Me})Ni_2(\mu\text{-}NO_2)]ClO_4$ (3-ClO_4): A solution of $NaNO_2$ (30 mg, 0.43 mmol) in water (1 mL) was added to a solution of complex **1**-ClO_4 (92 mg, 0.10 mmol) in methanol (30 mL). The color of the reaction mixture turned from yellow to green. After the mixture was stirred for 1 h solid $LiClO_4\cdot 3H_2O$ (160 mg, 1.00 mmol) was added. The solution was stirred for a further 2 h during which time an olive-green solid precipitated. The solid was isolated by filtration, washed with little methanol and dried in air. Yield: 83 mg (89%); m.p. 315–316°C. IR (KBr): $\tilde{\nu}$=1183 [$\nu(NO_2^-)$], 1094vs cm^{-1} [$\nu(ClO_4^-)$]; UV/Vis (CH_3CN): λ_{max} (ε)=623 (39), 1104 nm ($59\,M^{-1}cm^{-1}$); CV (CH_3CN, 295 K, 0.1 M nBu_4NPF_6, ν= 100 mV s^{-1}; E (V) vs SCE): $E^1_{1/2}$=+0.74 (ΔE_p 108 mV), E^2_{pa}=+1.44 (irr.). The tetraphenylborate salt, $[(L^{Me})Ni_2(\mu\text{-}NO_2)]BPh_4$ (**3**-BPh_4), was prepared by adding $NaBPh_4$ (342 mg, 1.00 mmol) to a solution of **3**-ClO_4 (93 mg, 0.10 mmol) in methanol (40 mL). Yield: 110 mg (96%); m.p. 306–308°C; elemental analysis calcd (%) for $C_{62}H_{84}BN_7Ni_2O_2S_2$ (1151.71): C 64.66, H 7.35, N 8.51, S 5.57; found: C 64.33, H 7.45, N 8.53, S 4.42; IR (KBr): $\tilde{\nu}$= 1182 [$\nu(NO_2^-)$], 733, 704 cm^{-1} [$\delta(BPh_4^-)$]; UV/Vis (CH_3CN); λ_{max} (ε)=621 (40), 1111 nm ($57\,M^{-1}cm^{-1}$).

$[(L^{Me})Ni_2(\mu\text{-}N_3)]ClO_4$ (4-ClO_4): A solution of NaN_3 (13 mg, 0.20 mmol) in H_2O (1 mL) was added to a solution of complex **1**-ClO_4 (92 mg, 0.10 mmol) in methanol (30 mL). The color of the reaction mixture turned from yellow to dark yellow. After the mixture was stirred for 2 h solid $LiClO_4\cdot 3H_2O$ (160 mg, 1.00 mmol) was added. The resulting yellow suspension was stirred for a further 1 h. The solid was isolated by filtration, washed with cold methanol and dried in air. The compound was recrystallized once from a mixed ethanol/acetonitrile solvent system. Yield: 74 mg (80%); m.p. 307–309°C; IR (KBr, cm^{-1}): $\tilde{\nu}$= 2059 vs [$\nu(N_3^-)$], 1094 vs [$\nu(ClO_4^-)$]; UV/Vis (CH_3CN): λ_{max} (ε)=672 (37), 1092 nm ($84\,M^{-1}cm^{-1}$); CV (CH_3CN, 295 K, 0.1 M nBu_4NPF_6, ν=100 mV s^{-1}; E(V) vs SCE): $E^1_{1/2}$=+0.58 (ΔE_p 91 mV), E^2_{pa}=+1.53 (irr.). The tetraphenylborate salt, $[(L^{Me})Ni^{II}_2(\mu_{1,3}\text{-}N_3)]BPh_4$ (**4**-BPh_4), was prepared by adding $NaBPh_4$ (0.10 g, 0.30 mmol) to a solution of **4**·ClO_4 (50 mg, 0.054 mmol) in methanol (50 mL). Yield: 61 mg (98%); m.p. 304-306°C (decomp); IR (KBr, cm^{-1}): $\tilde{\nu}$= 2058 vs [$\nu(N_3^-)$], 732, 704 m [$\delta(BPh_4^-)$]; elemental analysis calcd (%) for $C_{62}H_{84}BN_9Ni_2S_2$ (1147.72): C 64.88, H 7.38, N 10.98; found: C 64.72, H 7.61, N 11.07; UV/Vis (CH_3CN); λ_{max} (ε)=673 (45), 1094 nm ($102\,M^{-1}cm^{-1}$).

$[(L^{Me})Ni_2(\mu\text{-}N_3)]N_3$ (4-N_3): A solution of NaN_3 (39 mg, 0.60 mmol) in H_2O (1 mL) was added to a solution of **1**-ClO_4 (92 mg, 0.10 mmol) in methanol (30 mL). The color of the reaction mixture turned from yellow to dark yellow. After the mixture was stirred for 1 h it was filtered and left to stand for two days at room temperature during which time yellow needles of the title compound precipitated. This material was filtered, washed with methanol (1 mL) and dried in air. Yield: 44 mg (50%); m.p. 268°C (decomp); IR (KBr): $\tilde{\nu}$=2059, 2036 cm^{-1} [$\nu(N_3^-)$].

$[(L^{Me})Ni_2(\mu\text{-}N_2H_4)](ClO_4)_2$ (5-$(ClO_4)_2$): A solution of $N_2H_4\cdot H_2O$ (25 mg, 0.50 mmol) in H_2O (1 mL) was added to a solution of **1**·ClO_4 (92 mg, 0.10 mmol) in methanol (30 mL). The reaction mixture was stirred for 2 h during which time the color turned from yellow to green. Solid $LiClO_4\cdot 3\text{-}H_2O$ (160 mg, 1.00 mmol) was added. The suspension was stirred for a further 1 h to ensure complete precipitation of the title compound. The solid was isolated by filtration, washed with little cold methanol and dried in air. Yield 74 mg (73%), m.p. 310–311°C (decomp); IR (KBr): $\tilde{\nu}$= 3300 s, 3290 sh, 3248 cm^{-1} [$\tilde{\nu}$(NH)], 1093 vs [$\tilde{\nu}(ClO_4^-)$]; UV/Vis (CH_3CN); λ_{max} (ε)=624 (33), 1114 nm ($67\,M^{-1}cm^{-1}$); CV (CH_3CN, 295 K, 0.1 M nBu_4NPF_6, ν=100 mV s^{-1}; E(V) vs SCE): $E^1_{1/2}$=+0.90 (ΔE_p= 106 mV), E^2_{pa}=+1.56 (irr.); elemental analysis calcd (%) for $C_{38}H_{68}Cl_2N_8Ni_2O_8S_2$ (1017.42): C 44.86, H 6.74, N 11.01, S 6.30; found: C 45.02, H 6.72, N 11.03, S 6.03.

$[(L^{Me})Ni_2(\mu\text{-}pz)]ClO_4$ (6-ClO_4): A solution of pyrazole (13.6 mg, 0.200 mmol), triethylamine (20 mg, 0.20 mmol) and **1**-ClO_4 in methanol (30 mL) was stirred for 4 h. A solution of $LiClO_4\cdot 3H_2O$ (160 mg, 1.00 mmol) in methanol (1 mL) was added. The resulting pale green precipitate was filtered, washed with methanol and recrystallized from a mixed CH_3CN/C_2H_5OH (1:1) solution to give pale green crystals of the title compound. Yield 77 mg (81%); m.p. 332–333°C (decomp); IR (KBr, cm^{-1}): $\tilde{\nu}$=1092 vs [$\nu(ClO_4^-)$]; UV/Vis (CH_3CN): λ_{max} (ε)=382 (1880), 634 (24), 1178 (52) nm ($M^{-1}cm^{-1}$); CV(CH_3CN, 295 K, 0.1 M nBu_4NPF_6, ν=100 mV s^{-1}; E(V) vs SCE): $E^1_{1/2}$=+ 0.58 (ΔE_p 94 mV), $E^2_{1/2}$=+ 1.24 (ΔE_p 127 mV). The tetraphenylborate salt, $[(L^{Me})Ni^{II}_2(\mu\text{-}pz)]BPh_4$ (**6**-BPh_4), was prepared by adding $NaBPh_4$ (342 mg, 1.00 mmol) to a solution of **6**-ClO_4 (95 mg, 0.10 mmol) in methanol (50 mL). Yield: 61 mg (98%). An analytically pure sample was obtained by recrystallization from acetonitrile/ethanol (1:1). M.p. 308–309°C (decomp.); IR (KBr, cm^{-1}): $\tilde{\nu}$= 732, 704 m [$\delta(BPh_4^-)$]; UV/Vis (CH_3CN): λ_{max} (ε)=380 (2146), 634 (23), 1180 nm ($52\,M^{-1}cm^{-1}$); elemental analysis calcd (%) for $C_{65}H_{87}BN_8Ni_2S_2$ (1172.77): C 66.57, H 7.48, N 9.55, S 5.47; found: C 66.23, H 7.58, N 9.45, S 5.44.

$[(L^{Me})Ni_2(\mu\text{-}pydz)](ClO_4)_2$ (7-$(ClO_4)_2$): Solid $Pb(ClO_4)_2$ (80 mg, 0.20 mmol) was added to a solution of **1**-ClO_4 (92 mg, 0.10 mmol) in methanol (30 mL). The color of the reaction mixture turned from yellow to dark green. After the reaction mixture was stirred for 5 min it was filtered off from a white solid ($PbCl_2$). To the filtrate was added a solution of pyridazine (9.6 mg, 0.12 mmol) in acetonitrile (1 mL) to give a brown-yellow solution. The solution was kept at room temperature for two days during which time brown crystals of **7**-$(ClO_4)_2\cdot(CH_3CN)_2$ formed. The solid was isolated by filtration, washed with little methanol and dried in air. Yield: 46 mg (42%); m.p. 290–292°C (decomp); elemental analysis calcd (%) for $C_{42}H_{68}Cl_2N_8Ni_2O_8S_2\cdot H_2O$ (1083.48): C 46.56, H 6.51, N 10.34; found: C 45.92, H 6.73, N 9.83; IR (KBr, cm^{-1}): $\tilde{\nu}$= 1100 vs [$\nu(ClO_4^-)$]; UV/Vis (CH_3CN); λ_{max} (ε)=615 (66), 1095 nm ($62\,M^{-1}cm^{-1}$). CV(CH_3CN, 295 K, 0.1 M nBu_4NPF_6, ν=100 mV s^{-1}; E(V) vs SCE): $E^1_{1/2}$=+ 0.97 (irr.). The compound crystallizes with two molecules of acetonitrile of crystallization. The crystals lose these solvent molecules quickly when stored in air.

$[(L^{Me})Ni_2(\mu\text{-}phtz)](ClO_4)_2$ (8-$(ClO_4)_2$): This compound was prepared as before from **1**-ClO_4 (92 mg, 0.10 mmol), $Pb(ClO_4)_2$ (80 mg, 0.20 mmol), and phthalazine (16 mg, 0.12 mmol). The solution was kept at room temperature for two days during which time brown crystals of **8**-

$(ClO_4)_2 \cdot CH_3CN$ formed. The solid was isolated by filtration, washed with little methanol, and dried in air. This compound was recrystallized from a mixed acetonitrile/ethanol solvent system. Yield: 69 mg (62%); m.p. 316–318°C (decomp); elemental analysis calcd (%) for $C_{46}H_{70}Cl_2N_8Ni_2O_8S_2 \cdot H_2O$ (1115.52): C 48.74, H 6.40, N 9.89, S 5.66; found: C 48.66, H 6.51, N 9.81, S. 5.41; IR (KBr, cm^{-1}): $\tilde{\nu}$ = 1100 vs [$\nu(ClO_4^-)$]; UV/Vis (CH_3CN); λ_{max} (ε) = 629 (43), 1111 nm ($57\,M^{-1}\,cm^{-1}$). The compound crystallizes with one molecule of solvent of crystallization. The crystals lose the solvent molecules quickly when stored in air.

$[(L^{Me})Ni^{II}_2(\mu\text{-}OBz)]ClO_4$ (9-ClO_4): A colorless solution of sodium benzoate (29 mg, 0.20 mmol) in methanol (5 mL) was added to a yellow solution of **1**-ClO_4 (92 mg, 0.10 mmol) in methanol (15 mL) was added and the resulting green solution was stirred at room temperature for 30 min. Solid lithium perchlorate (160 mg, 1.00 mmol) was then added and the reaction mixture was stirred for a further 30 min. The resulting green precipitate was filtered off and washed with little methanol. Yield 77 mg (76%); m.p. >320°C; IR (KBr disk, cm^{-1}): $\tilde{\nu}$ = 1600 s, 1568 s [$\nu_{as}(CO_2)$], 1427 m [$\nu_s(CO_2)$]; UV/Vis (CH_3CN): λ_{max} (ε) = 650 (30), 1118 nm ($66\,M^{-1}cm^{-1}$). The tetraphenylborate salt, $[(L^{Me})Ni^{II}_2(\mu\text{-pz})]BPh_4$ (**6**-BPh_4), was prepared by adding $NaBPh_4$ (342 mg, 1.00 mmol) to a solution of **9**-ClO_4 (100 mg, 0.10 mmol) in methanol (50 mL). Yield 98 mg (80%); M.p. 168–170°C (decomp); elemental analysis (%) calcd for $C_{69}H_{89}BN_6Ni_2O_2S_2$ (1226.81): C 67.55, H 7.31, N 6.85, S 5.23; found: C 66.38, H 7.46, N 6.15, S 4.73; IR (KBr disk): $\tilde{\nu}$ = 1600, 1567 [$\nu_{as}(OBz^-)$], 1427 cm^{-1} [$\nu_s(OBz^-)$]; UV/Vis (CH_3CN): λ_{max} (ε) = 650 (32), 1121 ($67\,M^{-1}\,cm^{-1}$); UV/Vis (CH_2Cl_2): λ_{max} (ε) = 652 (38), 1118 ($71\,M^{-1}\,cm^{-1}$). This compound was additionally characterized by X-ray crystal structure analysis.

Exchange experiments: The relative stability constants of the nickel complexes **2**–**9** were determined by exchange experiments as described in Equation (2). The reactions were run at room temperature in a mixed acetonitrile/methanol (1:1) solvent system. In a typical experiment, 25 mL of a 0.5×10^{-3} M solution of the complex $[(L^{Me})Ni_2(\mu\text{-}L')]ClO_4$ in acetonitrile was treated with 25 mL of a 5.0×10^{-3} M solution containing the coligand L″ (i.e. $NaNO_3$, $NaNO_2$, NaN_3, NaOAc, NaOBz, $N_2H_4 \cdot H_2O$, pyridazine, phthalazine, pyrazole/triethylamine) in aqueous (5%) methanol. After the solution was stirred for 5 h, ethanol (50 mL) was added, and the volume was reduced in vacuum to about 5 mL. The resulting precipitate was isolated by filtration and dried in air. The presence or absence of $[(L^{Me})Ni_2(\mu\text{-}L')]ClO_4$ and $[(L^{Me})Ni_2(\mu\text{-}L'')]ClO_4$ in the product and their relative concentration was estimated by visual comparison of the IR spectrum of the product with those of the pure samples.

Physical measurements: Melting points were determined in capillaries and are uncorrected. IR spectra were taken on a Bruker VECTOR 22 FT-IR-spectrophotometer as KBr pellets. Electronic absorption spectra were recorded on a Jasco V-570 UV/Vis/NIR spectrophotometer. Cyclic voltammetry measurements were carried out at 25°C with an EG&G Princeton Applied Research potentiostat/galvanostat model 263 A. The cell was composed of a Pt working electrode, a Pt wire auxiliary electrode, and a Ag wire as reference electrode. Concentrations of solutions were 0.10 M in supporting electrolyte $[(n\text{Bu})_4N]PF_6$ and about 1×10^{-3} M in sample. Cobaltocene was used as internal standard with $E(Cp_2Co^+/Cp_2Co) = -1.345$ V versus Cp_2Fe^+/Cp_2Fe. All potentials were converted to the SCE reference using tabulated values.[82] Temperature-dependent magnetic susceptibility measurements on powdered solid samples were carried out on a SQUID magnetometer (MPMS Quantum Design) over the temperature range 2.0–300 K. The magnetic field applied was 0.2 T. The observed susceptibility data were corrected for the underlying diamagnetism by using Pascal's constants.

Crystal stucture determinations: Crystals of $[(L^{Me})Ni_2(NO_2)]ClO_4 \cdot MeOH$ (**3**-$ClO_4 \cdot MeOH$) suitable for X-ray crystallographic analysis were obtained by recrystallization from methanol. Crystals of $[(L^{Me})Ni_2(O_2NO)]$-$NO_3 \cdot H_2O \cdot MeOH$ (**2**-$NO_3 \cdot H_2O \cdot MeOH$), $[(L^{Me})Ni_2(N_3)]N_3 \cdot 3MeOH$ (**4**-$N_3 \cdot 3MeOH$), $[(L^{Me})Ni_2(pydz)](ClO_4)_2 \cdot 2MeCN$ (**7**-$(ClO_4)_2 \cdot (MeCN)_2$), and $[(L^{Me})Ni_2(\mu\text{-}N_2H_4)](ClO_4)_2$ (**5**-$(ClO_4)_2$) were taken from the reaction mixtures. Crystals of $[(L^{Me})Ni_2(pz)]BPh_4 \cdot MeCN$ (**6**-$BPh_4 \cdot MeCN$), $[(L^{Me})$-$Ni_2(phtz)](ClO_4)_2 \cdot EtOH$ (**8**-$(ClO_4)_2 \cdot EtOH$), and $[(L^{Me})Ni_2(OBz)]BPh_4$ (**9**-BPh_4), were grown by slow evaporation from an acetonitrile/ethanol mixed solvent system. The crystals were removed from the mother liquor and immediately immersed in a drop of perfluoropolyether oil. A suitable crystal was selected, attached to a glass fiber, and placed in a low-temperature nitrogen stream of the diffractometer. All data were collected at 210(2) K using a BRUKER AXS diffractometer (equipped with $Mo_{K\alpha}$ radiation and a CCD area detector). The ShelXTL version 5.10 program package was used for the structure solutions and refinements.[83] Absorption corrections were applied using the SADABS program.[84] The crystal structures were solved by direct methods and refined by full-matrix least-squares procedures. All non-hydrogen atoms were refined anisotropically except for the disordered NO_3^- counteranion and MeOH and H_2O solvate molecules in the crystal structure of **2**-$NO_3 \cdot MeOH \cdot H_2O$. Split atom models were used to account for disorder of *tert*-butyl groups in complexes **2**–**9**. The site occupancies of the two positions were refined as follows C32a–C34a/C32b–C34b: 0.54(3)/0.46(3) for **2**, 0.51(1)/0.49(1) for **4**, 0.58(1)/0.42(1) for **6**, 0.66(1)/0.34(1) for **9**; and C36a–C38a/C36b–C38b: 0.65(1)/0.35(1) for **3**; 0.57(1)/0.43(1) for **6**, 0.58(1)/0.42(1) for **7**, 0.52(1)/0.48(1) for **8**, and 0.67/0.33 for **9**. For **2**, the NO_3^- counteranion and the H_2O molecule of solvent of crystallization were found to be disordered over two positions. The site occupancies of the respective positions were fixed in each case at 0.50. For the nitrito-bridged complex **3**, the NO_2^- ligand was found to be disordered over the configurations: Ni1-N7(O2a)-O1-Ni2 and Ni1-O1-N7(O2b)-Ni2 at 0.84(1) and 0.15(1) occupancies, respectively. The site occupancy factors were refined subject to the condition that their sum equal unity. N7 and O1 were refined in the 85% orientation only. This did not introduce any noticeable anomalies in bond lengths or thermal parameters. The following molecules were also found to be disordered over two positions: in **4** one MeOH solvate (O3a-C41a/O3b-C41b) at 0.57(1)/0.43(1), in **7** one CH_3CN molecule (N10a-C45a-C46a/N10b-C45b-C46b) at 0.73(4)/0.27(4)), in **8** the two ClO_4^- ions (Cl1a-O1-O2-O3-O4/Cl1b-O1b-O2b-O3-O4b) at 0.72(1)/0.28(1) and Cl2-O5-O6a-O7a-O8a/Cl2-O5-O6b-O7b-O8b at 0.68(1)/0.32(1), and the EtOH solvate molecule C47-C48-O9a/C47-C48-O9b at 0.50/0.50 (fixed) occupancies. The high residual electron density in the crystal structure of **2**-$NO_3 \cdot MeOH \cdot H_2O$ is due to the disordered NO_3^- counteranion.

Hydrogen atoms were included in the refinement at calculated positions using a riding model included in the ShelXTL program. Hydrogen atoms were given isotropic thermal parameters 1.2 times (1.5 times for CH_3 groups) the thermal parameter of the atoms to which they were attached. The hydrogen atoms of the N_2H_4 group in **5** were calculated assuming a N–H distance of 0.96 Å and an ideal tetrahedral geometry. Selected details of the data collection and refinement are given in Table 3.

CCDC-223457–CCDC-223464 (**2**–**9**, respectively) contain the supplementary crystallographic data for this paper. These data can be obtained free of charge via www.ccdc.cam.ac.uk/conts/retrieving.html (or from the Cambridge Crystallographic Data Centre, 12 Union Road, Cambridge CB2 1EZ, UK (fax: (+44) 1223–336–033; or deposit@ccdc.cam.uk).

Acknowledgments

We are particularly grateful to Prof. Dr. H. Vahrenkamp for providing facilities for X-ray crystallographic measurements. Financial support of this work from the Deutsche Forschungsgemeinschaft (Priority programme "Molecular Magnetism", KE 585/4–1) and by the Wissenschaftliche Gesellschaft in Freiburg is gratefully acknowledged.

[1] D. J. Cram, M. J. Cram in *Container Molecules and Their Guests* (Ed.: J. F. Stoddart), The Royal Society of Chemistry, Cambridge, **1994**.
[2] a) F. Vögtle, *Supramolekulare Chemie*, Teubner, Stuttgart, **1992**; b) J. M. Lehn, *Supramolecular Chemistry*, Wiley, Chichester, **1995**; c) J. W. Steed, J. L. Atwood, *Supramolecular Chemistry*, Wiley, Chichester, **2000**.
[3] S. Hecht, J. M. J. Fréchet, *Angew. Chem.* **2001**, *113*, 76–94; *Angew. Chem. Int. Ed.* **2001**, *40*, 74–91.
[4] F. Hof, S. L. Craig, C. Nuckolls, J. Rebek, Jr., *Angew. Chem.* **2002**, *114*, 1556–1578; *Angew. Chem. Int. Ed.* **2002**, *41*, 1488–1508.
[5] J. W. Canary, B. C. Gibb, *Prog. Inorg. Chem.* **1997**, *45*, 1–83.
[6] D. V. Yandulov, R. R. Schrock, *Science* **2003**, *301*, 76–83.

[7] J.-U. Rohde, J.-H. In, M. H. Lee, W. W. Brennessel, M. R. Bukowski, A. Stubna, E. Münck, W. Nam, L. Que, Jr., *Science* **2003**, *299*, 1037–1039.

[8] a) M. T. Reetz, S. R. Waldvogel, *Angew. Chem.* **1997**, *109*, 870–873; *Angew. Chem. Int. Ed. Engl.* **1997**, *36*, 865–867; b) M. T. Reetz, *Catal. Today* **1998**, *42*, 399.

[9] E. Engeldinger, D. Armspach, D. Matt, *Angew. Chem.* **2001**, *113*, 2594–2597; *Angew. Chem. Int. Ed.* **2001**, *40*, 2526–2529.

[10] a) O. Seneque, M.-N. Rager, M. Giorgi, O. Reinaud, *J. Am. Chem. Soc.* **2001**, *123*, 8442–8443; b) Y. Rondelez, M.-N. Rager, A. Duprat, O. Reinaud, *J. Am. Chem. Soc.* **2002**, *124*, 1334–1340.

[11] B. R. Cameron, S. J. Loeb, G. P. A. Yap, *Inorg. Chem.* **1997**, *36*, 5498–5504.

[12] J. F. Stoddart, R. Zarzycki, *Recl. Trav. Chim. Pays-Bas* **1988**, *107*, 515-528.

[13] C. Wieser, C. B. Dieleman, D. Matt, *Coord. Chem. Rev.* **1997**, *165*, 93–161.

[14] a) P. Chaudhuri, K. Wieghardt, B. Nuber, J. Weiss, *Angew. Chem.* **1985**, *97*, 774–775; *Angew. Chem. Int. Ed. Engl.* **1985**, *24*, 778–779; b) P. Chaudhuri, K. Wieghardt, *Prog. Inorg. Chem.* **1988**, *35*, 329–436; c) A. Diebold, A. Elbouadili, K. S. Hagen, *Inorg. Chem.* **2000**, *39*, 3915–3923; d) W. B. Tolman, *Acc. Chem. Res.* **1997**, *30*, 227–237.

[15] a) N. Kitayima, W. B. Tolman, *Prog. Inorg. Chem.* **1995**, *43*, 419–531; b) S. Trofimenko, *Scorpionates: The Coordination Chemistry of Polypyrazolylborate Ligands*, Imperial College Press, London, UK, **1999**; c) S. Trofimenko, *Chem. Rev.* **1993**, *93*, 943–980; d) G. Parkin, *Adv. Inorg. Chem.* **1995**, *42*, 291–393.

[16] a) S. Herold, S. J. Lippard, *J. Am. Chem. Soc.* **1997**, *119*, 145–156; b) D. Lee, S. J. Lippard, *J. Am. Chem. Soc.* **1998**, *120*, 105–113; c) J. Du Bois, T. J. Mizoguchi, S. J. Lippard, *Coord. Chem. Rev.* **2000**, *200–202*, 443–485.

[17] J. R. Hagadorn, L. Que, Jr., W. B. Tolman, *J. Am. Chem. Soc.* **1998**, *120*, 13531–13532.

[18] J. B. Fontecha, S. Goetz, V. McKee, *Angew. Chem.* **2002**, *114*, 4735–4758; *Angew. Chem. Int. Ed.* **2002**, *41*, 4553–4556.

[19] a) A. J. Atkins, A. J. Blake, M. Schröder, *J. Chem. Soc. Chem. Commun.* **1993**, 1662–1665; b) A. J. Atkins, D. Black, A. J. Blake, A. Marin-Becerra, S. Parsons, L. Ruiz-Ramirez, M. Schröder, *Chem. Commun.* **1996**, 457–464; c) N. D. J. Branscombe, A. J. Blake, A. Marin-Becerra, W.-S. Li, S. Parsons, L. Ruiz-Ramirez, M. Schröder, *Chem. Commun.* **1996**, 2573–2574; d) N. D. J. Branscombe, A. J. Atkins, A. Marin-Becerra, E. J. L. McInnes, F. E. Mabbs, J. McMaster, M. Schröder, *Chem. Commun.* **2003**, 1098–1099.

[20] a) S. Brooker, P. D. Croucher, *J. Chem. Soc. Chem. Commun.* **1995**, 1493–1494; b) S. Brooker, P. D. Croucher, *J. Chem. Soc. Chem. Commun.* **1995**, 2075–2076; c) S. Brooker, P. D. Croucher, F. M. Roxburgh, *J. Chem. Soc. Dalton Trans.* **1996**, 3031–3037; d) S. Brooker, P. D. Croucher, *Chem. Commun.* **1997**, 459–460; e) S. Brooker, P. D. Croucher, T. C. Davidson, G. S. Dunbar, A. J. McQuillan, G. B. Jameson, *Chem. Commun.* **1998**, 2131–2132.

[21] N. H. Pilkington, R. Robson, *Aust. J. Chem.* **1970**, *23*, 2225–2236.

[22] a) P. A. Vigato, S. Tamburini, D. Fenton, *Coord. Chem. Rev.* **1990**, *106*, 25–170; b) D. Fenton, *Chem. Soc. Rev.* **1999**, *28*, 159–168.

[23] a) H. Okawa, H. Furutachi, D. E. Fenton, *Coord. Chem. Rev.* **1998**, *174*, 51–75; b) M. Shinoura, S. Kita, M. Ohba, H. Okawa, H. Furutachi, M. Suzuki, *Inorg. Chem.* **2000**, *39*, 4520–4526.

[24] a) C. Fraser, L. Johnston, A. L. Rheingold, B. S. Haggerty, G. K. Williams, J. Whelan, B. Bosnich, *Inorg. Chem.* **1992**, *31*, 1835–1844; b) B. Bosnich, *Inorg. Chem.* **1999**, *38*, 2554–2562; c) A. L. Gavrilova, C. J. Qin, R. D. Sommer, A. L. Rheingold, B. Bosnich, *J. Am. Chem. Soc.* **2002**, *124*, 1714–1722.

[25] H_2L^H: 3,6,9,17,20,23-hexaaza-29,30-dithiol-13,27-di(*tert*-butyl)tricyclo[23,3,$1^{11.15}$]triaconta-1(28),11,13,15(30),25,26-hexaene; H_2L^{Me}: 3,6,9,17,20,23-hexamethyl-3,6,9,17,20,23-hexaaza-29,30-dithiol-13,27-di(*tert*-butyl)tricyclo[23,3,$1^{11.15}$]triaconta-1(28),11,13,15(30),25,26-hexaene.

[26] a) B. Kersting, G. Steinfeld, *Inorg. Chem.* **2002**, *41*, 1140–1150; b) M. H. Klingele, G. Steinfeld, B. Kersting, *Z. Naturforsch. B* **2001**, *56*, 901–907.

[27] C. J. Harding, V. McKee, J. Nelson, Q. Lu, *J. Chem. Soc. Chem. Commun.* **1993**, 1768–1770.

[28] B. Kersting, G. Steinfeld, *Chem. Commun.* **2001**, 1376–1377.

[29] B. Kersting, *Angew. Chem.* **2001**, *113*, 4109–4112; *Angew. Chem. Int. Ed.* **2001**, *40*, 3987–3990.

[30] G. Steinfeld, V. Lozan, B. Kersting, *Angew. Chem.* **2003**, *115*, 2363–2365; *Angew. Chem. Int. Ed.* **2003**, *42*, 2261–2263.

[31] F. A. Cotton, G. Wilkinson, C. A. Murillo, M. Bochmann, *Advanced Inorganic Chemistry*, 6th ed., Wiley, New York, **1999**.

[32] For a complete listing of these IR absorptions see: Experimental part, Complex **2**.

[33] K. Nakamoto, *Infrared and Raman Spectra of Inorganic and Coordination Compounds*, 5th ed., VCH-Wiley, New York, **1997**.

[34] K. Wieghardt, H. Siebert, *Z. Anorg. Allg. Chem.* **1970**, *374*, 186–190.

[35] a) K.-H. Linke, F. Dürholz, P. Hädicke, *Z. Anorg. Allg. Chem.* **1968**, *356*, 113–117; b) K. Brodersen, *Z. Anorg. Allg. Chem.* **1957**, *290*, 24–34.

[36] D. Sellmann, P. Kreutzer, G. Huttner, A. Frank, *Z. Naturforsch. B* **1978**, *33*, 1341–1346.

[37] H. Lang, K. Köhler, L. Zsolnai, *Chem. Ber.* **1995**, *128*, 519–523.

[38] J. Hausmann, Diploma Thesis, University of Freiburg, Germany, May **2001**.

[39] B. Kersting, D. Siebert, *Inorg. Chem.* **1998**, *37*, 3820–3828.

[40] a) S. Brooker, *Coord. Chem. Rev.* **2001**, *222*, 33–56; b) S. Brooker, P. D. Croucher, T. C. Davidson, G. S. Dunbar, C. U. Beck, S. Subramanian, *Eur. J. Inorg. Chem.* **2000**, 169–179.

[41] a) D. Kong, A. E. Martell, R. J. Motekaitis, J. H. Reibenspies, *Inorg. Chim. Acta* **2001**, *317*, 243–251; b) D. Kong, A. E. Martell, J. Reibenspies, *Inorg. Chim. Acta* **2002**, 333, 7–14; c) J. Gao, A. E. Martell, J. Reibenspies, *Inorg. Chim. Acta* **2002**, *329*, 122–128; d) H. He, A. E. Martell, R. J. Motekaitis, J. H. Reibenspies, *Inorg. Chem.* **2000**, *39*, 1586–1592.

[42] G. J. Kleywegt, W. G. R. Wiesmeyer, G. J. Van Diel, W. L. Driessen, J. Reedijk, J. K. Noordik, *J. Chem. Soc. Dalton Trans.* **1985**, 2177–2184.

[43] H. Luo, J.-M. Luo, P. E. Fanwick, J. G. Stowell, M. A. Green, *Inorg. Chem.* **1999**, *38*, 2071–2078.

[44] L. Hausherr-Primo, K. Hegetschweiler, H. Rüegger, L. Odier, R. D. Hancock, H. W. Schmalle, V. Gramlich, *J. Chem. Soc. Dalton Trans.* **1994**, 1689–1701.

[45] C. A. Hunter, *Chem. Soc. Rev.* **1994**, *23*, 101–109.

[46] M. A. Hitchman, G. L. Rowbottom, *Coord. Chem. Rev.* **1982**, *42*, 55–132.

[47] A Sieker, A. J. Blake, B. F. G. Johnson, *J. Chem. Soc. Dalton Trans.* **1996**, 1419–1427.

[48] D. M. L. Goodgame, M. A. Hitchman, D. F. Marsham, *J. Chem. Soc. A* **1971**, 259–264.

[49] C. G. Pierpont, D. N. Hendrickson, D. M. Duggan, F. Wagner, E. K. Barefield, *Inorg. Chem.* **1975**, *14*, 604–610.

[50] P. Chaudhuri, M. Guttmann, D. Ventur, K. Wieghardt, B. Nuber, J. Weiss, *J. Chem. Soc. Chem. Commun.* **1985**, 1618–1620.

[51] J. Ribas, A. Escuer, M. Monfort, R. Vicente, R. Cortes, L. Lezama, T. Rojo, *Coord. Chem. Rev.* **1999**, *193–195*, 1027–1068.

[52] a) C. J. Harding, F. E. Mabbs, E. J. MacInnes, V McKee, J. Nelson, *J. Chem. Soc. Dalton Trans.* **1996**, 3227–3230; b) A. Escuer, C. J. Harding, Y. Dussart, J. Nelson, V McKee, R. Vicente, *J. Chem. Soc. Dalton Trans.* **1999**, 223–227.

[53] a) A. Escuer, R. Vicente, J. Ribas, M. S. El Fallah, X. Solans, M. Font-Bardia, *Inorg. Chem.* **1993**, *32*, 3727–3732; b) A. Escuer, R. Vicente, J. Ribas, M. S. El Fallah, X. Solans, M. Font-Bardia, *Inorg. Chem.* **1994**, *33*, 1842–1847.

[54] A. F. Hollemann, E. Wiberg, *Lehrbuch der Anorganischen Chemie*, 91.-100. ed., Walter de Gruyter, Berlin **1985**, p. 557–559.

[55] a) D. Sellmann, H. Kunstmann, F. Knoch, M. Moll, *Inorg. Chem.* **1988**, *27*, 4183–4190; b) D. Sellmann, W. Soglowek, F. Knoch, M. Moll, *Angew. Chem.* **1989**, *101*, 1244–1245; *Angew. Chem. Int. Ed. Engl.* **1989**, *28*, 1271–1272.

[56] a) R. A. Henderson, G. J. Leigh, C. J. Pickett, *Adv. Inorg. Chem. Radiochem.* **1983**, *25*, 197–292; b) D. Sutton, *Chem. Rev.* **1993**, *93*, 995–1022.

[57] a) D. Sellmann, K. Engl, F. W. Heinemann, J. Sieler, *Eur. J. Inorg. Chem.* **2000**, 1079–1089; b) K. Matsumoto, T. Koyama, Y. Koide, *J. Am. Chem. Soc.* **1999**, *121*, 10913–10923; c) S. Matsukawa, S.

Kuwata, Y. Ishii, M. Hidai, *J. Chem. Soc. Dalton Trans.* **2002**, 2737–2746.
[58] a) L. Blum, I. D. Williams, R. R. Schrock, *J. Am. Chem. Soc.* **1984**, *106*, 8316–8317; b) R. C. Murray, R. R. Schrock, *J. Am. Chem. Soc.* **1985**, *107*, 4557–4558.
[59] J. W. Steed, J. L. Atwood, *Supramolecular Chemistry*, Wiley, Chichester, **2000**, p. 175.
[60] J. Reedijk, in *Comprehensive Coordination Chemistry, Vol. 2*, (Eds.: G. Wilkinson, R. D. Gillard, J. A. McCleverty), Pergamon Press, New York, **1987**, p. 73–98.
[61] T. L. Gilchrist, *Heterocyclic Chemistry*, Longman Scientific & Technical, Essex, **1987**.
[62] a) A. M. Barrios, S. J. Lippard, *J. Am. Chem. Soc.* **2000**, *122*, 9172–9177; b) A. M. Barrios, S. J. Lippard, *Inorg. Chem.* **2001**, *40*, 1250–1255.
[63] The reactions could not be monitored by UV/Vis spectroscopy. The spectral changes were too insensitive for some of the reactions.
[64] This finding could result from the different solubilites of the two species in question. To eliminate this possibility, the reactions were also monitored by infrared spectroscopy (in CH_2Cl_2) solution. This gave the same ordering of the coligands.
[65] N. N. Greenwood, A. Earnshaw, *Chemie der Elemente*, VCH, Weinheim, **1988**, p. 1210.
[66] From the pK_a values of the corresponding acids [pK_a(BzOH) = 4.22, pK_a(AcOH) = 4.75], the acetate ion is a stronger base than the benzoate group, and hence a stronger σ-donor ligand (it has a higher affinity for the proton), see: N. Isaacs, *Physical Organic Chemistry*, 2nd ed., Addison Wesley Longman, Essex, **1996**.
[67] We have determined the relative stability constants of the corresponding zinc complexes $[(L^{Me})Zn^{II}_2(\mu\text{-}OBz)]ClO_4$ (**9′**) and $[(L^{Me})Zn^{II}_2(\mu\text{-}OAc)]ClO_4$ (**10′**) by NMR spectroscopy. A 0.10 mL portion of a 2.0×10^{-2} M solution of sodium acetate in CD_3OD was added to 1.00 mL of a 2.0×10^{-3} M solution of **10′** in CD_3OD. The solution was stirred for 1 min and transferred to an NMR tube. The temperature was held constant at 300 K. The relative concentrations of **10′** and **9′** were determined by integration of the signals for the *tert*-butyl protons at $\delta = 1.24$ ppm (for **10′**) and at $\delta = 0.95$ ppm (for **9′**), yielding a ratio of 0.30 to 0.70. The relative stability constant can be calculated by using the following expression: $K_{rel} = [\mathbf{10'}][OAc^-]/[\mathbf{9'}][OBz^-] = 5.4(1)$, showing that the benzoate complex is about one order of magnitude ($\Delta G = -4.2$ kJ mol^{-1}) more stable than the acetate complex.
[68] In view of the analytical data, the presence of a small amount of a dinuclear nickel species containing the azide in the $\mu_{1,1}$-bridging mode (which can be expected to have an $S = 2$ ground state) can also be invoked to explain the magnetic behavior in the low temperature region. This would be in good agreement with the analytical data. Furthermore, this could also explain the decrease of the $\chi_M T$ values at very low temperatures. It can be interpreted in terms of the zero-field splitting of the $S = 2$ ground state of the $\mu_{1,1}$-azido bridged nickel complex.
[69] C. J. O′Connor, *Prog. Inorg. Chem.* **1982**, *29*, 203–283.
[70] A. P. Ginsberg, R. L. Martin, R. W. Brookes, R. C. Sherwood, *Inorg. Chem.* **1972**, *11*, 2884–2889.
[71] O. Kahn, *Molecular Magnetism*, VCH, Weinheim, **1993**.
[72] T. Beissel, T. Glaser, F. Kesting, K. Wieghardt, B. Nuber, *Inorg. Chem.* **1996**, *35*, 3936–3947.
[73] K. K. Nanda, A. W. Addison, N. Paterson, E. Sinn, L. K. Thompson, U. Sakaguchi, *Inorg. Chem.* **1998**, *37*, 1028–1036.
[74] F. Meyer, A. Jacobi, B. Nuber, P. Rutsch, *Inorg. Chem.* **1998**, *37*, 1213–1218.
[75] $\chi_{dim} = (Ng^2\mu_B{}^2/kT)[2\exp(2J/kT) + 10\exp(6J/kT)]/[1 + 3\exp(2J/kT) + 5\exp(6J/kT)]$, $\chi_{mono} = 2Ng^2\mu_B{}^2/3kT$.
[76] a) J. B. Goodenough, *Phys. Rev.* **1955**, *100*, 564–573; b) J. Kanamori, *J. Phys. Chem. Solids* **1959**, *20*, 87–98; c) A. P. Ginsberg, *Inorg. Chim. Acta Rev.* **1971**, *5*, 45–68.
[77] B. Kersting, G. Steinfeld, D. Siebert, *Chem. Eur. J.* **2001**, *7*, 4253–4258.
[78] a) T. Beissel, F. Birkelbach, E. Bill, T. Glaser, F. Kesting, C. Krebs, T. Weyhermüller, K. Wieghardt, C. Butzlaff, A. X. Trautwein, *J. Am. Chem. Soc.* **1996**, *118*, 12376–12390; b) U. Bossek, D. Nühlen, E. Bill, T. Glaser, C. Krebs, T. Weyhermüller, K. Wieghardt, M. Lengen, A. X. Trautwein, *Inorg. Chem.* **1997**, *36*, 2834–2843.
[79] Y. Elerman, M. Kabak, I. Svoboda, H. Fuess, K. Griesar, W. Haase, *Z. Naturforsch. B* **1996**, *51*, 1132–1136.
[80] J. Ribas, M. Montfort, I. Resino, X. Solans, P. Rabu, F. Maingot, M. Drillon, *Angew. Chem.* **1996**, *108*, 2671–2673; *Angew. Chem. Int. Ed. Engl.* **1996**, *35*, 2520–2522.
[81] a) A. Escuer, R. Vicente, M. S. El Fallah, J. Ribas, X. Solans, M. Font-Bardía, *J. Chem. Soc. Dalton Trans.* **1993**, 2975–2976; b) R. Vicente, A. Escuer, J. Ribas, M. S. El Fallah, X. Solans, M. Font-Bardía, *Inorg. Chem.* **1995**, *34*, 1278-1281; c) J. Ribas, M. Montfort, B. K. Ghosh, R. Cortés, X. Solans, M. Font-Bardía, *Inorg. Chem.* **1996**, *35*, 864-868.
[82] N. G. Connelly, W. E. Geiger, *Chem. Rev.* **1996**, *96*, 877-910.
[83] ShelXTL version 5.10: Bruker AXS, Madison, WI, **1998**.
[84] SADABS, an empirical absorption correction program part ot the SAINTPlus NT version 5.0 package, BRUKER AXS, Madison, WI, **1998**.

Received: November 10, 2003 [F5705]